

SCF/SCFR signaling plays an important role in the early morphogenesis and neurogenesis of human embryonic neural retina

Yu Gong^{1,2}, Xiangyu He², Qiyu Li^{1,2}, Juncai He^{1,2}, Baishijiao Bian^{1,2}, Yijian Li^{1,2}, Linlin Ge^{1,2}, Yuxiao Zeng^{1,2}, Haiwei Xu^{1,2,*} and Zheng Qin Yin^{1,2,*}

ABSTRACT

The stem cell factor receptor (SCFR) has been demonstrated to be expressed in the neural retina of mice, rat and human for decades. Previous reports indicated that the SCFR correlates with glia differentiation of late retinal progenitor cells (RPCs), retinal vasculogenesis and homeostasis of the blood-retinal barrier. However, the role of SCF/SCFR signaling in the growth and development of the neural retina (NR), especially in the early embryonic stage, remains poorly understood. Here, we show that SCF/SCFR signaling orchestrates invagination of the human embryonic stem cell (hESC)-derived NR via regulation of cell cycle progression, cytoskeleton dynamic and apical constriction of RPCs in the ciliary marginal zone (CMZ). Furthermore, activation of SCF/SCFR signaling promotes neurogenesis in the central-most NR via acceleration of the migration of immature ganglion cells and repressing apoptosis. Our study reveals an unreported role for SCF/SCFR signaling in controlling ciliary marginal cellular behaviors during early morphogenesis and neurogenesis of the human embryonic NR, providing a new potential therapeutic target for human congenital eye diseases such as anophthalmia, microphthalmia and congenital high myopia.

KEY WORDS: Embryonic stem cells (ESCs), SCFR, Retina, Growth, Development

INTRODUCTION

The eye is the most important sensory organ that receives and transduces light signals to the visual cortex. Functional visual organs require specific morphological structures and appropriate size control. During early embryogenesis, the retinal neuroepithelium, which arises from the retinal anlage, evaginates laterally from the diencephalic wall to form an optic vesicle (OV). The distal region of the OV then invaginates to form a cup-like structure, the optic cup (OC), with the neural retina (NR) and the retinal pigment epithelium (RPE) being the inner and outer walls, respectively. Any abnormalities of these sequential steps of OC

morphogenesis leads to severe eye diseases such as anophthalmia, microphthalmia and coloboma (Heavner and Pevny, 2012).

Invagination of the NR is crucial for OC formation (Fuhrmann, 2010). Recent studies of the self-organized OC from human embryonic stem cells (hESCs) suggested that OC formation is a spontaneous process that consists of three consecutive local processes (relaxation of the NR, apical constriction of the hinge region and tangential expansion) (Eiraku et al., 2012). Adjacent to the hinge region where invagination of the NR occurs is the ciliary marginal zone (CMZ), which serves as a stem cell pool for *de novo* retinal neurogenesis during vertebrate eye development (Bélanger et al., 2017; Fischer et al., 2013; Kuwahara et al., 2015).


The stem cell factor (SCF) receptor SCFR, also known as KIT or CD117, is a 145 kDa transmembrane tyrosine kinase encoded by the SCFR proto-oncogene and is essential for gametogenesis, hematopoiesis and melanogenesis (Lennartsson and Rönstrand, 2012). Its specific inhibitors, such as imatinib, have been well applied in the treatment of chronic myelogenous leukemia (CML) and acute lymphocytic leukemia (AML) for decades. The SCFR and SCF are expressed in both peripheral nervous system (PNS) and central nervous system (CNS), and are involved in the survival, proliferation, differentiation and maturation of neural stem cells (NSCs) (Das et al., 2005a). Das et al. reported that SCFR expression is upregulated in ciliary epithelium (CE) NSCs *in vitro*, suggesting that signaling mediated by the SCFR may represent a mechanism used by stem cells in the optic neuroepithelium (Das et al., 2005b). In addition, the SCFR is thought to be involved in the organization of the neural tube and the brain (Keshet et al., 1991). However, the role of SCF/SCFR signaling in the growth and development of the NR, especially in the early embryonic stage, remains poorly understood.

The majority of previous reports about OC morphogenesis are based on research on the mouse retina. Our understanding of human embryonic retina development is limited by ethical constraints. Recently, OCs were self-organized from both the ESCs and induced pluripotent stem cells (iPSCs) via a stepwise method, which opened the door to achieving high fidelity in simulating human retina development and served as an ideal disease model *in vitro* (Eiraku et al., 2011; Kuwahara et al., 2015; Nakano et al., 2012; Paşca, 2018; Rossi et al., 2018).

Here, we have used the self-organized OCs from hESCs to investigate the biological function of SCF/SCFR signaling during early development of the human embryonic NR. We demonstrate that SCF/SCFR signaling facilitates human NR invagination by accelerating cell cycle progression of retinal progenitor cells (RPCs), regulating cytoskeleton dynamics and enhancing the apical constriction in the CMZ. In addition, we found that the activation of SCF/SCFR signaling produced a premature neuro-retina in the central

¹Southwest Hospital/ Southwest Eye Hospital, Third Military Medical University (Army Medical University), Chongqing 400038, PR China. ²Key Lab of Visual Damage and Regeneration & Restoration of Chongqing, Chongqing 400038, PR China.

*Authors for correspondence (xuhaiwei@tmmu.edu.cn; qinzqin@aliyun.com)

 Y.G., 0000-0003-2190-0369; X.H., 0000-0001-8115-3727; Q.L., 0000-0002-9355-2319; B.B., 0000-0002-0729-1555; Y.L., 0000-0002-7619-8207; L.G., 0000-0002-1797-3752; Y.Z., 0000-0003-1471-9887; H.X., 0000-0003-4828-579X; Z.Q.Y., 0000-0002-4253-7485

NR (cNR) by promoting the migration of immature ganglion cells and repressing cellular apoptosis.

RESULTS

Generation of hESC-derived OC with the CMZ

To recapitulate human embryonic retinal development with the least amount of extrinsic factors, we used the NR selective protocol previously described by Kuwahara et al. (2015). Dissociated hESCs (Line H1 WA01) were first reaggregated in a low-cell-adhesion V-bottom 96-well plate (10,000 cells/well). Embryonic bodies were induced by transient early treatment of BMP4 at day (D)6 in suspended culture and more than 4.16% further developed into a patterned layered retinal morphology with pigment accumulation by D24 (Fig. 1A). The qRT-PCR analysis showed the loss of pluripotency (downregulation of OCT4) and specification of the eye field (upregulation of Rax, Pax6 and Lhx2) of hESC aggregates after 24 days of differentiation (Fig. S1A). Retinal organoids acquiring a two-domain morphology consisting of the NR and RPE at D24 were collected and depicted as the OC (Fig. 1B). The eye field transcription factor Rax and NR progenitor markers Chx10 and Sox2 were restricted in the apical layer of the thick NR region, while the RPE progenitor marker MITF was restricted to the thin RPE region (Fig. 1C-E). Pax6 was expressed throughout the NR and across the NR-RPE junction, whereas the pluripotent marker SSEA4 was negative in the OC (Fig. 1D,E). The majority of cells in the OC were positive for the mitotic marker Ki67 (Fig. S1B,C). In the NR region, Ki67 was mainly located in the Chx10⁺ RPCs on the apical side of NR (Fig. S1L), while the basal side was occupied by nestin-positive radial glia, such as neural progenitor cells (Fig. S1J, K). The CMZ emerged as a tapering region directly adjacent to the pigment-accumulated RPE domain (Fig. 1F-H). In contrast to the

cNR region, which comprised a dense apical layer and a loose basal layer, there was only one compact cell layer in the tapering CMZ (Fig. S1D,E). Ki67⁺ cells were sparsely distributed in the distal tip of the CMZ but became dense in the proximal subdomain (Fig. S1F). The expression of P27kip1, the CDK inhibitor that positively controls cell cycle exit (Dyer and Cepko, 2001), was absent in the CMZ (Fig. S1G). The specific molecular marker of the ciliary margin SSEA1 (Koso et al., 2008) was expressed in the Chx10⁺ domain (Fig. 1I, Fig. S1H), while the pigmented ciliary epithelium marker AQP1 (Yamaguchi et al., 2006) was expressed only in the MITF⁺ domain adjacent to the junction (Fig. S1I). These data demonstrate a well-established human OC derived from hESCs that is characterized by classical morphology, including the CMZ.

The SCFR is strongly expressed and spatiotemporally confined in the CMZ of the human OC

The SCFR is distributed in multiple systems of vertebrate organisms, but limited information is available regarding its expression in the CNS (Lennartsson and Rönstrand, 2012). To determine the expression pattern of the SCFR during development of the human retina, we detected the SCFR signal by immunostaining OCs at different stages. During the induction of human OC, the SCFR first emerged at the outer region of embryonic bodies at D6, gradually enriched at the epithelium-like cells at D12 (Fig. S2B), and robustly located at the optic vesicle at D18 (Fig. S2A-C). At D24, the primary time of OC formation (Nakano et al., 2012), the SCFR was specifically expressed in the whole NR, with strong labeling at the NR-RPE border, but completely negative in the RPE (Fig. 2A,B). The SCFR⁺ region of the NR could be segregated into two parts: a central Sox2⁺/SCFR^{dim} domain and a peripheral Sox2⁻/SCFR^{strong} domain (Fig. 2A; Fig. S6C), which was characterized

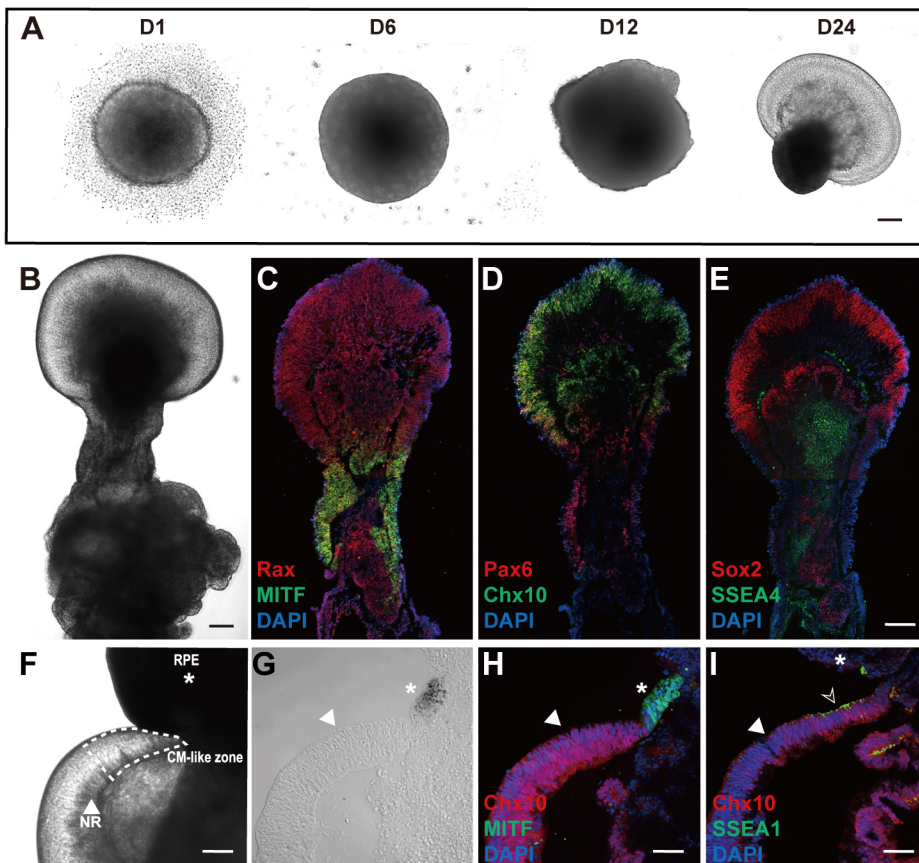


Fig. 1. Generation of hESC-derived OCs with the CMZ. (A) Phase-contrast microscopy images of the 3D human OC at different developmental time points [day (D)1, D6, D12 and D24], showing the sequential morphological changes from embryonic body (D1) to OC (D24). (B-E) Bright-field view (B) of 3D human OCs at D24 and immunostaining for Rax and MITF (C), Pax6 and Chx10 (D), and Sox2 and SSEA4 (E), indicating the successful differentiation of 3D OCs with both the NR (Rax, Pax6, Chx10, Sox2, SSEA4) and the RPE (MITF). (F,G) Phase-contrast microscopy images of OCs at D30 show the typical morphology of the wedge-like CMZ and its unique location between the NR (white triangle) and RPE (asterisk). (H) NR and RPE could be specifically stained with Chx10 (NR marker, red) and MITF (RPE marker, green) with a significant border. (I) The limit of CMZ and NR is well depicted by the double staining for SSEA1 and Chx10. White triangle, NR; asterisk, RPE; blank arrowhead, CMZ. Scale bars: 50 μ m in F-I; 100 μ m in A-E.

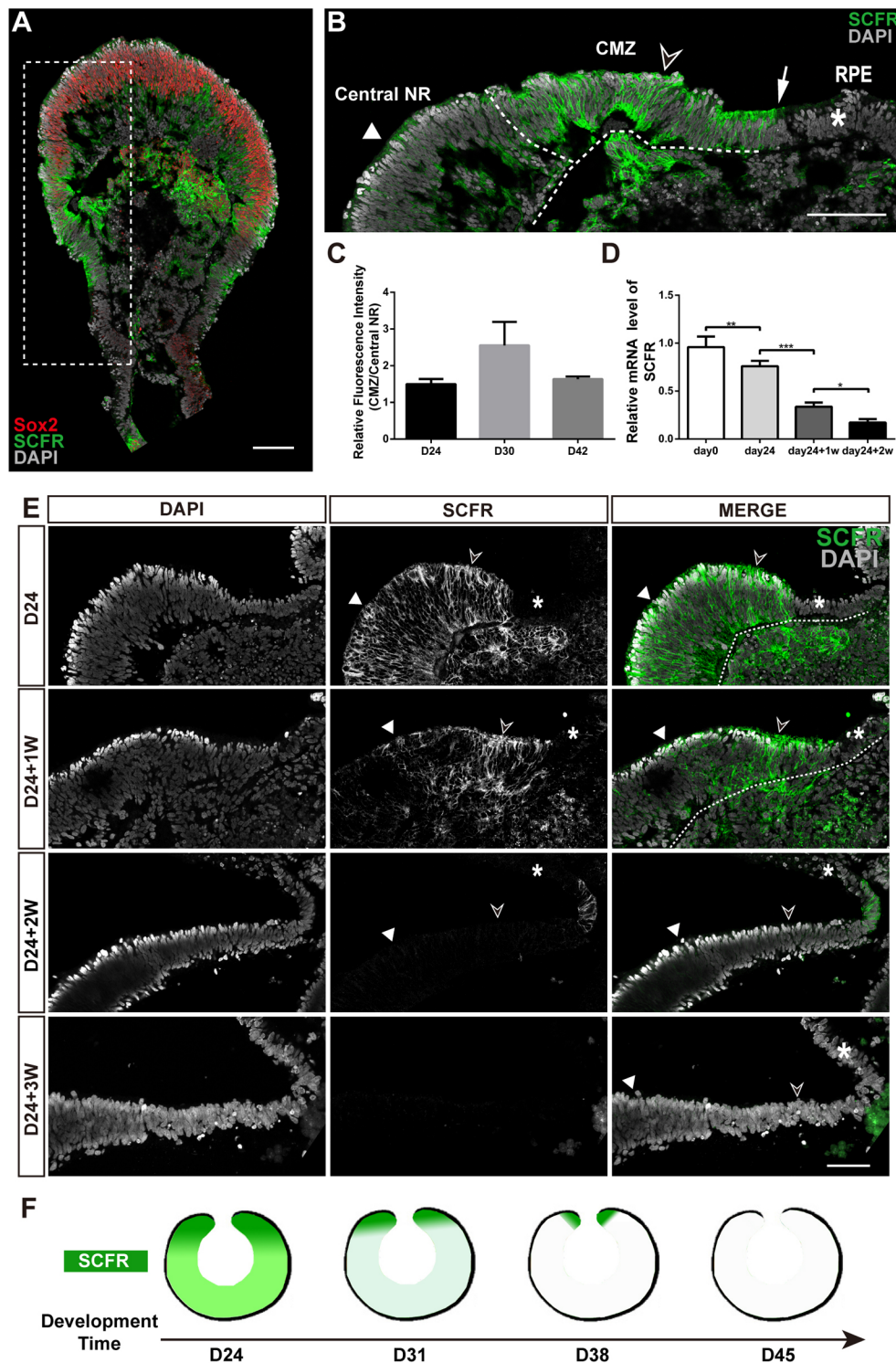


Fig. 2. The SCFR is strongly expressed and spatiotemporally confined in the CMZ of the human OC.

(A,B) Immunostaining of the 3D human OC at day (D) 24 for the SCFR and Sox2. B is a magnification of the region outlined in A. Sox2 mainly distributed in the nonmarginal NR, while the SCFR was expressed in the whole NR (white triangle) and CMZ (open arrowhead), but not in the RPE (asterisk). (C) Relative fluorescence intensity of the SCFR of the CMZ versus central NR, showing an ~1.5-2.5 times higher fluorescence intensity in the CMZ than in the central NR. Data are mean±s.d.; n=9 for each time point, three independent experiments. (D) RT-PCR analysis of the 3D human OC from D0 to D38, showing the timely downregulation of SCFR expression in the 3D OC. Data are mean±s.d.; n=9 for each time point, three independent experiments. (E) Immunostaining of the SCFR in the 3D human OC at D24, D31, D38 and D45. The expression of the SCFR in the NR was confined to the CMZ in a temporal-spatial manner and diminished at D45. White triangle, NR; asterisk, RPE; open arrowhead, CMZ. (F) Schematic of SCFR expression in the 3D human OC described in D. **P*<0.05, ***P*<0.01; ****P*<0.005. Scale bars: 100 μm.

as the tapering monolayered CMZ (Bélanger et al., 2017). The gray intensity of the SCFR signal in the CMZ is almost 1.5- to 2.5-fold higher than that in the nonmarginal NR at each developmental time point (Fig. 2C), indicating that the SCFR is strongly expressed in the CMZ in a spatially dynamic pattern. At D31 [D24+1 week (W)], the expression of the SCFR remained strong in the CMZ but gradually reduced in the nonmarginal NR. At D38 (D24+2W), the SCFR remained only at the most distal tip of the CMZ or the NR-RPE junction. By ~D45 (D24+3W), the whole OC tissue had lost SCFR expression, and only part of nonretinal tissue around the OC

maintained a relatively low expression of the SCFR (Fig. 2E). Consistently, the mRNA level of the SCFR determined by qRT-PCR analysis also showed a continuous decrease depending on the developmental stage of OC from D24 to D45 (Fig. 2D). Thus, the SCFR is strongly expressed and confined in the CMZ of hESCs-derived OCs in a spatiotemporal manner (Fig. 2F). On the other hand, SCF, the ligand of the SCFR, was not robustly expressed in the basal side of the central SCFR-positive NR until D18 when the original optic vesicle formed (Fig. S2A-E). Consistently, the phosphorylation of the SCFR emerged at the basal side of the cNR as well as remained

at a relatively low level in the CMZ (Fig. S2H,K). Taken together, these results demonstrated that SCF/SCFR signaling plays a role in the early development of human NR.

Activation of SCF/SCFR signaling facilitates NR invagination and increases axial length

SCF/SCFR signaling plays important roles in cell migration, proliferation and differentiation in the CNS (Matsui et al., 1990). The strong expression of the SCFR in the CMZ raised the issue of what role it may play in the development of the human OC. To

address this, we administered SCF, the ligand of the SCFR, and its inhibitor *isck03* to the 3D developing OC from D24 to D30, at which time the primary OC is formed (Fig. 3A). In the control condition, the NR-RPE angles were mainly obtuse ($104.0 \pm 4.3^\circ$) at D24 when the two-domain NR-RPE retinal organoid primarily formed. As development proceeded to D38, majority of the NR-RPE angle gradually became acute ($58.3 \pm 6.2^\circ$). The perpendicular angle ($90.8 \pm 4.1^\circ$) was somehow an intermediate state around D31 (Fig. 3B,C). Notably, the variability of the NR-RPE angle between D24 and D30 remarkably increased after SCF administration,

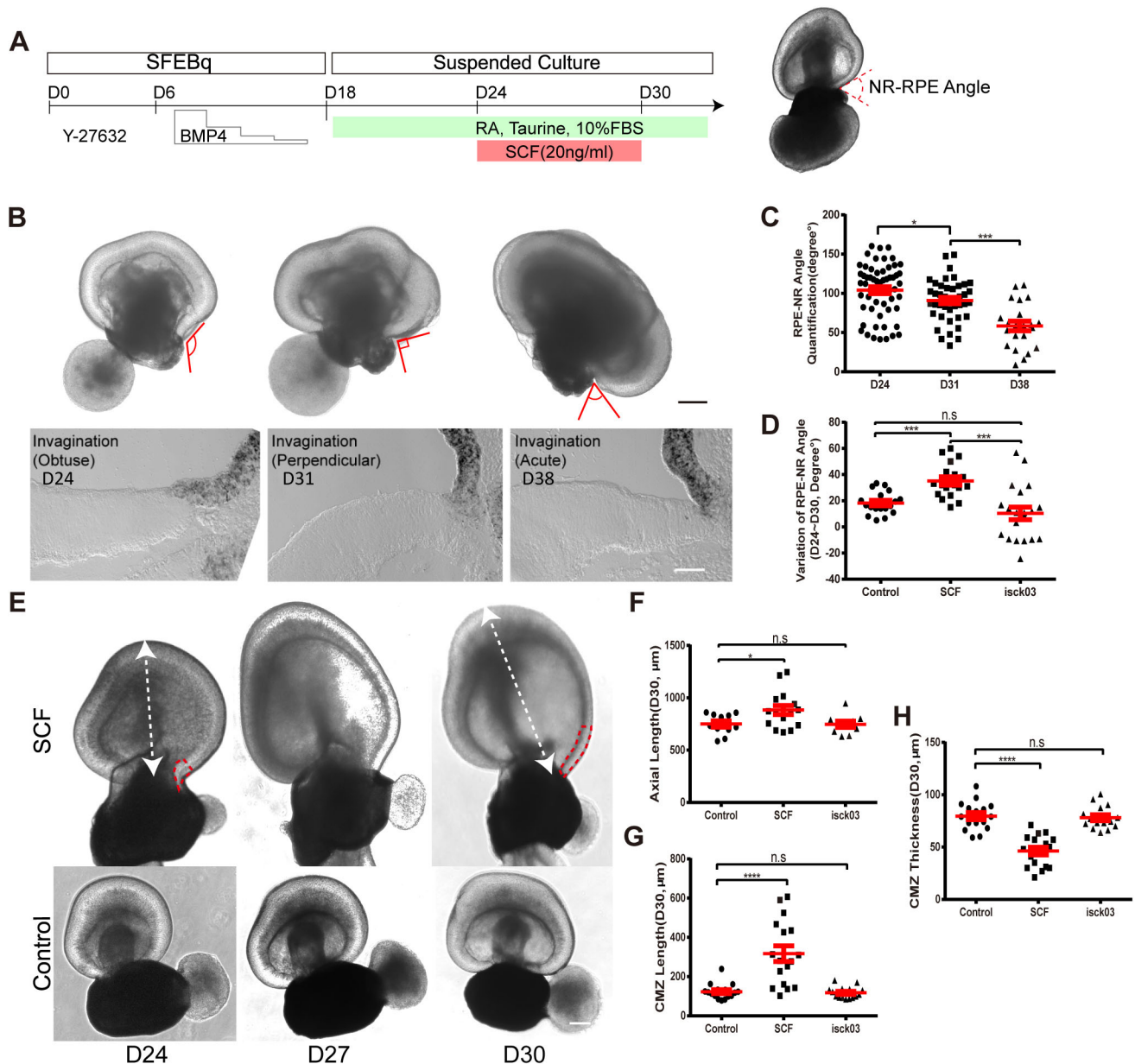


Fig. 3. Activation of SCF/SCFR signaling facilitates NR invagination and increases the axial length. (A) Schematic of the experiment protocol of SCF treatment of the 3D human retinal organoid culture. (B) Representative phase-contrast image of the 3D human optic with obtuse, perpendicular and acute NR-RPE angles, showing invagination of the NR during OC morphogenesis. (C) The quantification of the NR-RPE angle for each analyzed stage independently ($n=59$, 42 and 22 at each time point from three independent experiments). (D) The variability of NR-RPE angle of control, SCF and *isck03* group between day (D) 24 and D30 ($n=18$, 18 and 20 for each group from four independent experiments). (E) Phase-contrast images of the 3D human OC with and without SCF treatment at D24, D27 and D30. The white dashed line indicates the axial length. The dashed red line outlines the shape of CMZ. (F-H) Quantification analysis of the axial length ($n=11$, 16 and 9), CMZ length ($n=16$, 17 and 15) and CMZ thickness ($n=16$, 15 and 15) of OCs, showing that SCF treatment significantly increased the axial length and the CMZ length. Data are mean \pm s.e.m. and are collected from three independent experiments. * $P < 0.05$, *** $P < 0.005$, **** $P < 0.001$ (independent sample *t*-test). Scale bars: 50 μ m in B; 100 μ m in E.

suggesting that SCF/SCFR signaling might positively participate in invagination of the NR. However, it shows that there is a balance, as *isck03* seems to reduce the angle but not completely (Fig. 3D), and the presence of SCF has the opposite effect. In addition, we observed that the CMZ began to transform into an elongated and wedge-like morphology from the third day of SCF administration, while the CMZ of the control group remained short and column like. On the 6th day of SCF treatment, the CMZ had further elongated and exhibited a slim spindle-like sharp tapering shape (Fig. 3E). The axial length of the SCF-treated OC was also 100 μm longer than that of the control group. Moreover, the SCF-treated CMZ became significantly longer and thinner (Fig. 3G,H), suggesting that the expansion of CMZ may contribute to overgrowth of the axial length. In addition, we found the extended expression of SSEA1 in the SCF-treated CMZ and loss of SSEA1 expression in the *isck03*-treated CMZ (Fig. S3A-C). These results indicated that SCF/SCFR signaling is involved in the development of CMZ.

SCF/SCFR signaling orchestrates the cell cycle progression in the CMZ

Cell proliferation is the key internal driving force during invagination of the NR (Sasai, 2013). Hence, we sought to investigate the influence of SCF/SCFR signaling on the proliferation of CMZ-RPCs. To achieve this, we performed a pulse-labeling experiment using nucleotide analogues BrdU (Fig. 4A). The cell cycle length of the RPCs in the CMZ is less than 24 h (Fig. S4A-C) and most of the Ki67⁺ cells in the CMZ exited the cell cycle after one round of the cell cycle within 24 h (Fig. S4G). Moreover, the entrance or exit of the cell cycle seems to be independent of SCF/SCFR signaling, as neither SCF nor *isck03* treatment produced a significant difference in the proportion of BrdU⁺/Ki67⁺ cells in the BrdU⁺ cells and Ki67⁺ cells in the total cells 24 h after BrdU incorporation (Fig. S4H,I). However, the proportion of BrdU⁺/Ki67⁺ cells in the CMZ were markedly reduced by SCF treatment and increased when *isck03* (the SCFR inhibitor) was administered at the intermediate stage (12 h after BrdU incorporation) (Fig. S4J). This suggested that SCF may shorten the cell cycle length of RPCs and that inhibition of the SCFR prolonged the cell cycle (although it was still within 24 h). To verify this result, OCs were incubated with BrdU in the presence of SCF or *isck03* for 12 h (Fig. 4C,D). Compared with the control group, the accumulation of BrdU in the CMZ was greatly enhanced by SCF treatment. As a contrast, the *isck03* did not perturb the BrdU accumulation of RPCs (Fig. 4D,F). To further confirm this result, we performed a BrdU dilution experiment (Fig. 4A). The 24 h exposure of 3D OCs to BrdU heavily labeled the progenitor cells in the CMZ (Fig. 4B,E). As shown in the control group, BrdU⁺ cells in the CMZ were diluted after an additional 72 h (+96 h), and 21.1 \pm 1.8% of CMZ-RPCs remained BrdU positive. Surprisingly, BrdU⁺ cells in the CMZ following SCF treatment were largely diluted, and fewer CMZ-RPCs remained BrdU positive. In addition, the treatment of *isck03*, the specific inhibitor of the SCFR, reversed this accelerated dilution phenomenon, leaving ~41.4% BrdU⁺ cells in the CMZ (Fig. 4B,E). As no cell apoptosis was observed in the CMZ (Fig. 6S), the more BrdU was diluted, the more cycles the cells have gone through, which confirmed the accelerated cell cycling by SCF. Taken together, these results demonstrated that SCF/SCFR signaling orchestrates the cell cycle progression of RPCs, thus modulating the cell dynamics in the CMZ and further contributing to the morphogenesis of the NR.

Given that the central-peripheral (horizontal) orientation of cell division is highly correlated with the symmetric division in the

developing retina (Agathocleous and Harris, 2009; Cayouette and Raff, 2003; Das et al., 2003; Zhong and Chia, 2008; Žigman et al., 2005), the tangentially elongated CMZ after SCF treatment suggested that SCF/SCFR signaling might expand the stem cell pool via promotion of symmetric division of CMZ-RPCs. To further reveal the effect of SCF/SCFR signaling on the mode of CMZ-RPC division, we analyzed the spindle orientation of CMZ-RPCs by p-vimentin and Ki67 labeling (Fig. 4G). We observed the mixed orientation of division in the CMZ and the cNR. In the control group, we observed mainly horizontal orientation (47%) with some oblique (28%) and vertical (25%) orientation, indicating a robust symmetric division in the CMZ (Fig. 4H). However, in the cNR, 38% of cell divisions were horizontal, 26% were oblique and 36% were vertical (Fig. 4I), suggesting an increased tendency towards asymmetric division in the cNR, as described in previous reports (Harris and Perron, 1998; Larsen et al., 2009). Nevertheless, the perturbation of SCF/SCFR signaling did not alter the pattern of spindle orientation in both the CMZ and the cNR (Fig. 4H,I). These results indicated that the SCF/SCFR signaling orchestrates the cell cycle progression in the CMZ to produce a tangentially biased driving force within the internal CMZ, contributing to invagination of NR and the increased axial length.

SCF/SCFR signaling regulates cytoskeleton dynamics and apical constriction of the CMZ

The accelerated invagination of NR prompted us to address the issue of whether SCF/SCFR signaling regulates the mechanical dynamics of NR to facilitate deformation. To achieve this, we analyzed the cytoskeleton dynamics of NR by detecting F-actin assembly/disassembly by phalloidin staining because apical F-actin regulates the exocytosis of cells and alters the construction of extracellular matrix to change the tissue rigidity during rapid expansion of the apical surface (Wang et al., 2013). Cellular cytoskeletons of apical cells lost their continuous expression in the nonmarginal NR after SCF treatment and disassembled in the CMZ compared with the control group, which exhibited a more continuous F-actin construction (Fig. 5A,B). Disassembly of F-actin made the CMZ tissue more flexible and facilitated folding toward the RPE in this region, contributing to morphogenesis of the optic cup according to a previous atomic force microscopy analysis of the 3D neural retina (Eiraku et al., 2011). However, the treatment of *isck03* kept the integrity of F-actin both in the CMZ and central NR (Fig. 5C), demonstrating an active role for the SCFR in the cytoskeleton dynamic of NR. To investigate the driving force facilitating the invagination of the NR, we further examined actomyosin activity of the RPE-NR junction by immunostaining of phosphorylated myosin light chain 2 (pMLC) because invagination of the NR depends strongly on the fold direction, as evagination will occur if the NR folds in the opposite direction. Surprisingly, pMLC activity was significantly stronger after SCF treatment than in the control group in the apical CMZ but remained unchanged in the nonmarginal NR and relatively weak in the *isck03* treatment group (Fig. 5D,E,F). This result strongly indicates that SCF/SCFR signaling robustly enhances the activity of pMLC in the apical CMZ, which pulls the NR toward the RPE, thus accelerating the formation of an acute angle between the RPE and the apical surface of the NR. As inhibition of myosin activity may disrupt polarity of the apically convex Chx10⁺ epithelium of 3D retinal organoids (Lowe et al., 2016), we performed ZO-1 staining to assess the apical-basal polarity of the NR after SCF treatment. Consistent with the control group, ZO-1 was continuously located on the surface of

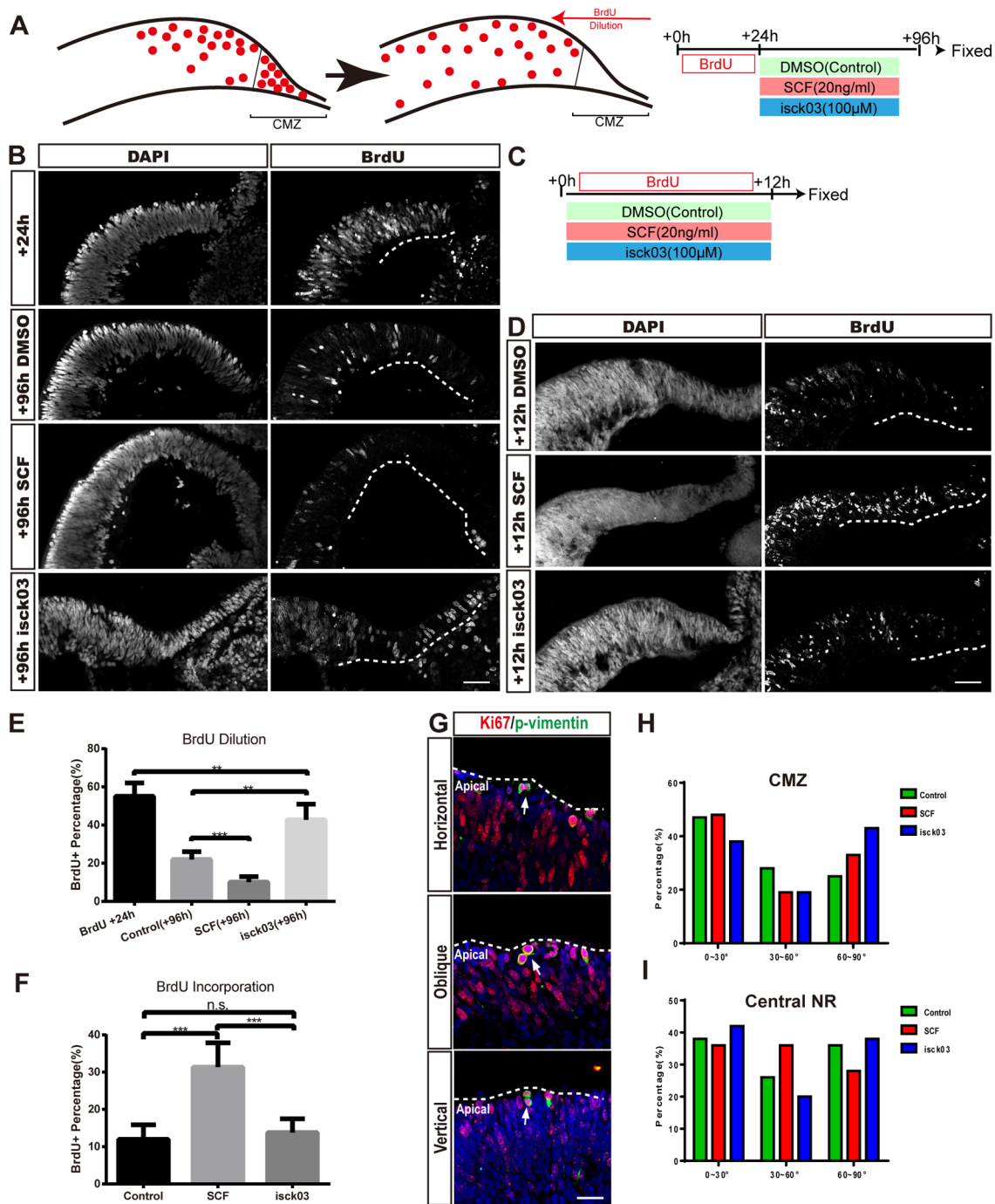


Fig. 4. SCF/SCFR signaling orchestrates the cell cycle progression in the CMZ. (A) Schematic of BrdU dilution experiment in 3D human retinal organoids. SCF, the SCFR ligand, and isck03, the SCFR inhibitor were administered for 72 h after BrdU withdrawal. (B) Immunostaining of the 3D OC for BrdU showing BrdU was abundant after incubation for 24 h and was more rapidly diluted by SCF treatment in the subsequent 72 h. Dashed line indicates the CMZ. (C) Schematic of the BrdU incorporation experiment in 3D human OC. (D) Immunostaining of the 3D OCs for BrdU after incubation for 12 h with SCF or isck03 treatment. SCF treatment robustly increased BrdU incorporation in the CMZ and isck03 treatment produced the opposite result. (E) Quantification of BrdU⁺ cells showing the BrdU dilution in the control and SCF treatment groups. Data are mean±s.e.m.; n=6 BrdU 24 h, n=12 controls, n=25 SCF, n=12 isck03, three independent experiments. (F) Quantification of BrdU⁺ cells for BrdU incorporation in the control and SCF treatment group. Data are mean±s.e.m.; n=18 controls, n=12 SCF, n=12 isck03, three independent experiments. Data are mean±s.e.m. Independent sample *t*-test. ***P*<0.01; ****P*<0.005. (G) Double staining of Ki67 and p-vimentin shows the typical spindle orientation (white arrows) of RPC mitotic divisions in the NR at D30. Scale bars: 50 μm in B,E; 20 μm in G. (H,I) Analysis of different spindle orientation in the CMZ and NR indicated that both the CMZ and central NR exhibit a mixture of three types of mitotic division and this is not altered by the administration of SCF and isck03 (*P*>0.05, 2×3 Fisher's exact test, n=81 for control, n=71 for SCF, n=106 for isck03, three independent experiments).

the outer cell layer of the NR after SCF and isck03 treatment, indicating that SCF/SCFR signaling does not affect NR polarity (Fig. 5G-I). Thus, SCF/SCFR signaling regulates cytoskeleton

dynamics and apical constriction of the CMZ to facilitate invagination of the NR, thereby accelerating formation of an acute angle between the RPE and the apical NR.

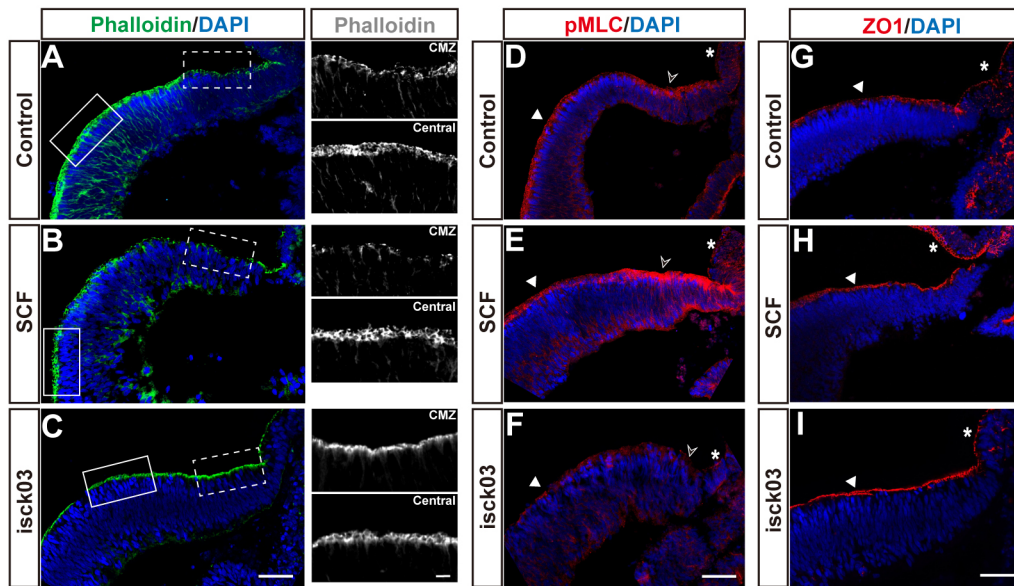


Fig. 5. SCF/SCFR signaling regulates cytoskeleton dynamics and apical constriction of the CMZ. (A-C) Immunostaining for F-actin using phalloidin of the 3D OC of the control, SCF and isck03 group at day (D) 30. Magnifications of the CMZ (top) correspond to the region of the white dashed box and magnifications of the central NR region (bottom) correspond to the region of the white solid box. F-actin in the control and isck03 group was kept in a continuous manner both in the CMZ and the central NR, while the SCF group was distributed in a noncontinuous manner in the CMZ and in a continuous but loose manner in the central NR. (D-F) Immunostaining of the 3D OCs at D30 for pMLC, showing that SCF treatment enhanced the activity of pMLC in the CMZ during invagination of the NR and isck03 decreased the activity of pMLC. The white triangle indicates the apical activity of pMLC in the CMZ. (G-I) Immunostaining for ZO-1 of the 3D OCs at D30, showing that SCF and isck03 administration did not change the polarity of the NR. White triangle, NR; asterisk, RPE; open arrowhead, CMZ. Scale bars: 50 μ m; 10 μ m at higher magnification.

Activation of SCF/SCFR signaling promotes the migration of immature ganglion cells, represses cellular apoptosis and produces a premature neuro-retina

In the human fetal eye, the differentiation of ganglion cells and cone photoreceptor cells begins in the central-most NR and eventually gives rise to the fovea (O'Brien et al., 2003). We found that the OCs of the SCF treatment group usually had a much thicker compacted inner cell layer in the central-most NR than that in the control and isck03 group (Fig. 6A,B,I,J). The thickened inner cell layers of the NR were contained numerous Pax6⁺, Brn3b⁺ and p27kip1⁺ cells (Fig. 6C-H), which mark naïve ganglion cells, the first-born NR cell lineage (located in the inner cell layers) (Cayouette et al., 2006). This finding led us to investigate the migration of naïve ganglion cells, because the apical-basal migration of naïve neurons is essential for neurogenesis and lamination in the CNS (Xu et al., 2015). Tuj1⁺ ganglion cells emerged in the nonmarginal NR and migrated from the apical region toward the basal side along the processes of Nestin⁺ radial glia-like cells (Fig. S1B,J,K). Surprisingly, significantly more Tuj1⁺ ganglion cells migrated in the outer cell layer of the central-most NR following SCF treatment (Fig. 6K,M-R). However, this phenomenon was defective in the isck03-treated NR (Fig. 6K,Q,R). Moreover, the number of cleaved-caspase 3⁺ apoptotic cells was dramatically decreased in the SCF-treated NR and increased in the isck03-treated group (Fig. 6L,S-U). The enhanced migration of immature ganglion cells and the repressed apoptosis by SCF treatment together suggest that SCF/SCFR signaling may also play a role in the development of the ganglion cell layer and the formation of the retinal neural circuit. To further explore whether SCF/SCFR signaling is involved in the production of the presence progenitors, we further analyzed multiple committed retinal progenitor/precursor cells marker such as islet 1 (ganglion cell progenitor/precursor cell), Crx (photoreceptor progenitor/precursor cell), calretinin (interneuron

progenitor/precursor cell) and CRALBP (Müller progenitor/precursor cell) in the central NR. During vertebrate retina development, six types of neuron and one type of glia are generated in a conserved order: ganglion cells were generated first, and rods, bipolar cells and Müller glia were produced last (Livesey and Cepko, 2001). These committed progenitor cells were sparsely generated by the retinal organoid at D30 (Fig. S5A,D,G,J,M,N). The induction of SCF promoted the genesis of islet 1⁺, calretinin⁺ and CRALBP⁺ progenitor/precursor cells but did not affect the production of Crx⁺ photoreceptor progenitor cells (Fig. S5B,E,H,K,M,N). Similarly, the treatment of isck03 remarkably increased the amount and proportion of all the committed progenitor/precursor cells (Fig. S5C,F,I,L-N). This result indicated that the imbalance of the SCF/SCFR signaling disturbed the early development of NR and result in a premature neuro-retina. It is worth mentioning that the mechanism underlying the pre-mature effect of SCF and isck03 on the NR development might be complex as there was a differential production bias in the photoreceptor, interneuron and neuroglia progenitor/precursor cells (Fig. S5M,N). As for the actively proliferating cells in the CMZ, they were not directed to produce terminally differentiated postmitotic cells (Kuwahara et al., 2015). Similarly, we did not observe any positive signal of these committed presence progenitor/precursor cells in our experiment. To summarize, all the above data supported the hypothesis that the SCF/SCFR plays an important role in the early neurogenesis of NR.

DISCUSSION

Organogenesis of the vertebrate eye is a multistep process that starts with the formation of optic vesicles followed by invagination of the distal optic vesicle, resulting in morphogenesis of the OC. Many congenital eye disorders, including anophthalmia, microphthalmia, coloboma and retinal dysplasia, stem from disruptions in the

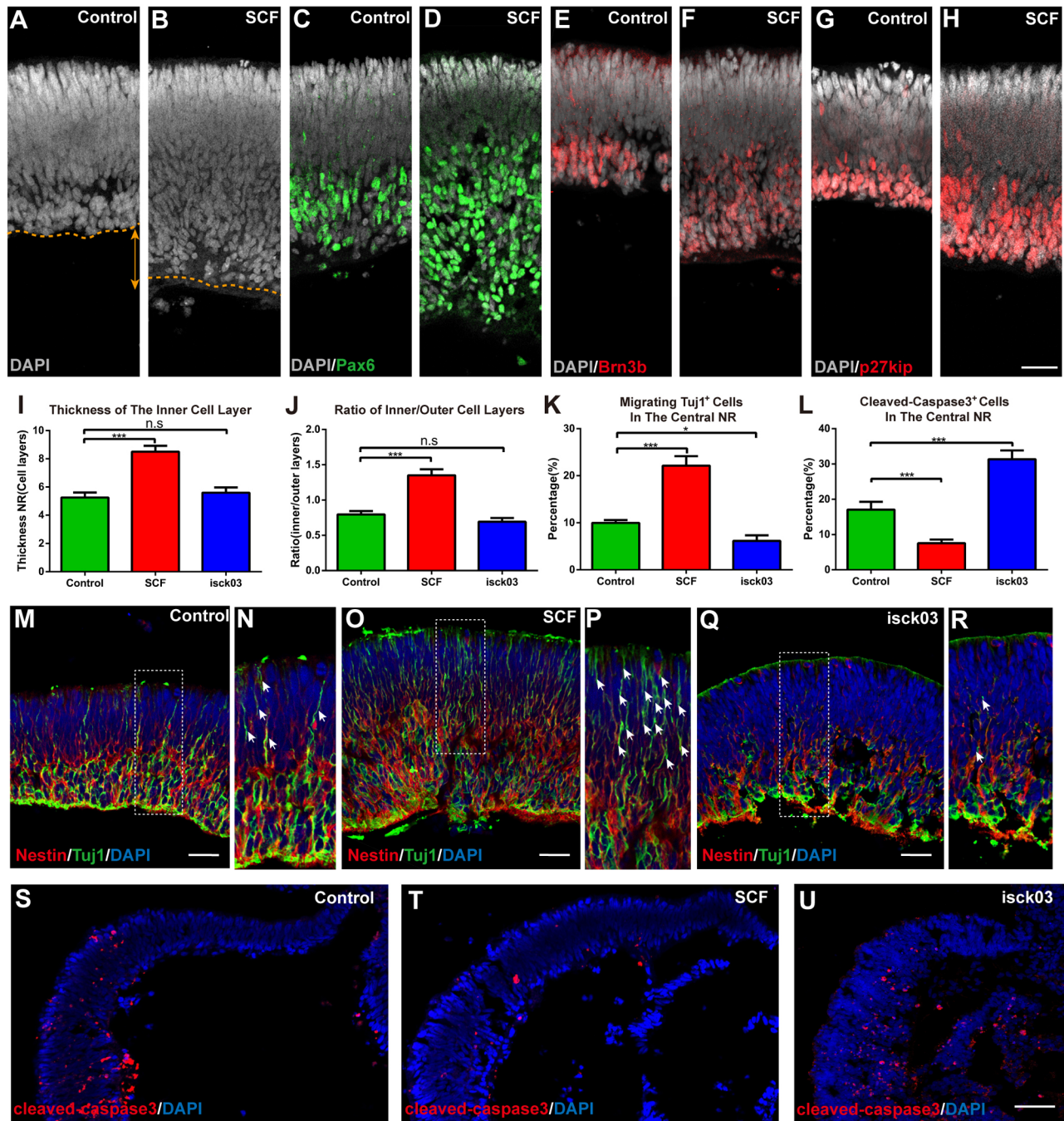


Fig. 6. SCF/SCFR signaling accelerates the migration of immature ganglion cells and represses cellular apoptosis in the nonmarginal NR. (A,B) DAPI staining of the central-most NR at day (D) 30 showing thickening of the inner cell layer after SCF treatment. Brown dashed line and double-headed arrow indicate the difference in the inner cell layer thickness. (C-H) Immunostaining of the central-most NR at D30 for Pax6 (C,D), Brn3b (E,F) and P27kip1 (G,H), showing robust accumulation of postmitotic ganglion cells in the inner cell layer. Scale bar: 25 μ m. (I,J) Quantification of the cell layers of the nonmarginal NR at D30 showing that SCF administration promoted the accumulation of cells in the inner cell layer. Data are mean \pm s.e.m., $n=9$ controls, $n=9$ SCF for each group, three independent experiments. (K) Quantification of the migrating Tuj1⁺ ganglion cells at D30 in the central NR showing that SCF administration robustly promoted the accumulation of cells in the inner cell layer while isck03 blocks the migration. Data are mean \pm s.e.m.; $n=9$ controls, $n=9$ SCF for each group, three independent experiments. (L) Quantification of cleaved caspase3⁺ apoptotic cells in the NR in control, SCF-treated and isck03-treated NR. Data are mean \pm s.e.m.; $n=9$ controls, $n=9$ SCF, $n=9$ isck03, three independent experiments. * $P<0.05$, *** $P<0.005$ (independent sample *t*-test). (M-R) Immunostaining for nestin and Tuj1 in the central-most NR at D30. (N,P,R) Magnifications of the regions indicated by the dashed boxes in M,O,Q, respectively. Significantly more Tuj1⁺ ganglion cells migrated in the NR in the SCF-treated group than in the control group. Fewer Tuj1⁺ ganglion cells were observed in the isck03-treated NR. White arrows indicate the migrating Tuj1⁺ cells. (S-U) Immunostaining of the NR for cleaved caspase 3 showing that cell apoptosis in the NR was dramatically repressed by SCF inducement (T) and deteriorated by isck03 administration (U). Scale bars: 50 μ m.

formation of the embryonic eye (Fuhrmann, 2010). How the unique shape of the OC is determined has remained an intriguing matter for many decades. Several extrinsic and intrinsic determinants, such as

fibroblast growth factors (FGFs), bone morphogenetic proteins (BMPs) and retinoic acid (RA) have been identified to contribute to the specification and morphogenesis of the OC (Chen et al., 2013;

Heermann et al., 2015; Picker and Brand, 2005; Valdivia et al., 2016). However, we still suffer from a huge lack of understanding about the mechanism of OC formation.

Expanding and integrating existing knowledge of the molecular and genetic machinery underlying retinal development is crucial not only for elucidating normal developmental mechanisms but also for developing therapeutic interventions aimed at vision restoration (Bassett and Wallace, 2012). Determining the mechanism of OC morphogenesis in human fetal eyes, however, has been difficult due to stringent ethical limitations. In recent years, researchers have established several protocols to culture 3D retinal organoids from hESCs or iPSCs to obtain qualified laminated 3D retinal tissue and functional photoreceptors with an outer segment (Eiraku et al., 2011; Nakano et al., 2012; Zhong et al., 2014). Combining these advanced techniques, we showed that SCF/SCFR signaling regulates proliferation, cytoskeleton assembly and apical constriction dynamics of RPCs in the CMZ of 3D human OCs, orchestrating invagination of the NR and axial growth of the OC. SCF/SCFR signaling also facilitated neurogenesis of the inner neuroblast cell layers in the central-most NR via promotion of immature ganglion cell migration and repressing cellular apoptosis, indicating that SCF/SCFR signaling plays a position-dependent role in the development of the human embryonic eye. Although SCF/SCFR signaling has been widely investigated in the tumorigenesis of acute myeloid leukemia (AML), melanoma and gastrointestinal stromal tumors (GISTs), no reports have discussed the role of SCF/SCFR signaling in human embryonic eye development (Heinrich et al., 2002; Hirota et al., 1998; Woodman and Davies, 2010).

In this study, we showed that SCFR expression was expressed throughout the NR and gradually confined in the CMZ in a spatiotemporal manner (Fig. 2C). As for the human embryonic retina, the SCFR was expressed both in the central NR and far peripheral NR, and reached the highest level during 7th to 12th gestation week (Hasegawa et al., 2008; Zhou et al., 2015). The developmental stage of 3D retinal organoid may be ~3–4 weeks earlier than human developing retina based on the expression time of Chx10 in a recent report on the integrated transcriptional analysis of the developing human retina (Fig. S2G) (Mellough and Bauer, 2019). The time-dependent difference and the defective periocular tissue in the retinal organoid may together contribute to the differential expression of the SCFR between the retinal organoid and fetal eye. Moreover, this result is in contradiction with the expression pattern of the SCFR in the mouse retina, in which the SCFR is peaking at P0 and located in the central-most NR and expands toward the peripheral region except for the CMZ (Koso et al., 2007), indicating that the species difference cannot be ignored on the expression and function of the SCFR.

The existence of niche-like ciliary marginal zone of vertebrate embryonic neuro-retina was identified in mouse and human retinal organoids recently (Bélangier et al., 2017; Kuwahara et al., 2015). A previous report proposed that the actively proliferating cells in the CMZ produce progenitors *de novo* by continuous cell division. Meanwhile, according to our data, the proportion of proliferating cells in the CMZ remained constant and no sign of apoptosis was observed in the CMZ at the early development stage of retinal organoid (Fig. S4I,K; Fig. 6S). These results suggested that there might be a dynamic balance between the proliferation of stem cells and migration of progenitor cells in the CMZ, which may be orchestrated by the SCF/SCFR signaling pathway. Moreover, heterogeneity of ciliary marginal cells should also be considered as we found that the CMZ could actually be subdivided into two parts: a more peripheral Chx10⁺/Sox2⁻ domain and a central

Chx10⁺/Sox2⁺ domain (Fig. S6C,D). This division pattern is reminiscent of the CMZ in the amphibian and fish retina, which consists of the slowly dividing uncommitted stem cells in the far peripheral region, committed rapidly dividing progenitors in the central CMZ and differentiated neurons at the central edge of the CMZ (Harris and Perron, 1998; Xue and Harris, 2012). On the other hand, the spindle oriental in the CMZ is mixed with horizontal, oblique and vertical division mode (Fig. 4G-I). This result further confirmed the cell heterogeneity in the CMZ. Our data revealed the function in regulating the cell cycle length of the SCF/SCFR signaling, which might contribute to the heterogeneity in the CMZ as disturbed cell cycle length of neural progenitors alter cell fate in the developing CNS (Pilaz et al., 2016). A conditional SCFR knockout hESC cell line and detailed single-cell sequencing analysis of CMZ will be needed in future research.

The invagination of NR is most crucial step in the morphogenesis of two wall-like OC. As the unique anatomy region between the rigid RPE and relaxed NR, the CMZ is poorly discussed in this important morphological event. As we have reported, the role of orchestrator in the cellular dynamics of CMZ endows SCF/SCFR signaling with the power to drive the change of shape. On the other hand, SCF/SCFR signaling facilitates CMZ deformation by upregulating apical constriction and disassembling the cytoskeleton of apical cells. Sasai and his colleagues have reported that pMLC activity completely disappears in the 3D human OC (Nakano et al., 2012). However, in their model, a whole invaginated NR encapsulated in an intact outer RPE tissue emerged on D24, while our model underwent a delayed invagination process from D24 to D38. The expression of SCF in adjacent RPE suggested that RPE served as a supporting tissue for the CMZ by providing SCF (Fig. S2E), which indicated the prolonged invagination may result from the polarized distribution of RPE and NR of our retinal organoids. More interestingly, compared with the phosphorylation level of the SCFR in the central NR, the activation of the SCFR was always relatively limited in the CMZ, even though the exogenous SCF was added (Fig. S2I,L). This is contradictory to the high expression of the SCFR in the CMZ. We speculate that the activation of the SCFR in the CMZ is more complex than that in the central NR. Co-activation with other receptors or cell-cell contact activation of the SCFR in the CMZ should be considered in future investigations (Lennartsson and Rönstrand, 2012; Mellough et al., 2015; Oakie et al., 2019).

From fish to mammals, the RGC has consistently been shown to be the earliest retinal cell type generated by RPCs occupying the inner neuroblast cell layer (Heavner and Pevny, 2012). In the CNS, nestin⁺ neural stem cells construct a scaffold-like structure, which provides a path for Tuj1⁺ neurons to climb from the apical side toward the basal side of the neural epithelium (Xu et al., 2013, 2015). Moreover, previous reports have shown that SCFR signaling can promote the migration and axonal extension of the CNS neurons (Gujjarro et al., 2013; Sun et al., 2004). Here, we have identified a similar pro-migration effect of SCF/SCFR signaling on RGC generation in the central-most region of the NR, which might further develop into the fovea (Hoshino et al., 2017). In addition, we found that cellular apoptosis in the NR was dramatically repressed after activation of the SCFR and this result could be antagonized by a SCFR inhibitor. During development of the retina, far more neurons are generated than are ultimately needed, with almost one half of them undergoing programmed cell death shortly before establishing meaningful contacts within their targets (Vecino and Acera, 2015). This repression of apoptosis could further perturb the normal development of neural circuit formation and disturb cell death-

related morphogenesis, resulting in congenital amblyopia, optic nerve hypoplasia or even retina degeneration (Teng and Toyama, 2011; Toyama et al., 2008). Considering the important function of migration, cell cycle length and apoptosis in the genesis of neuro-retina, the SCF/SCFR signaling may exert multiple functions and mechanisms in the neurogenesis and morphogenesis of the human embryonic eye by connecting multiple fundamental cell behaviors.

The relevance of the SCFR to translational medicine is also of great interest. As a cell-surface antigen, the SCFR could be used to sort retinal progenitor cells for cell therapy of retinal degeneration such as the retinitis pigmentosa (RP) disease. The SCFR⁺ donor cells survive up to 6 months in the subretinal space of host retina without generating teratoma. More importantly, in addition to robust material transfer and perfect cell replacement, these donor cells greatly inhibit the activation of microglia cells and improve the immune microenvironment of the RP disease (Chen et al., 2016; Zou et al., 2019). Our data well support the idea of SCFR⁺ RPCs from a developmental view, and partially explain the advantages for transplantation, such as retinal multipotency, limited proliferation, strong survivability and proper migration. In addition to the role in the light-sensing neuro-retina, we demonstrated that SCF/SCFR signaling orchestrates the cell cycle progression in the CMZ to increase the axial length at the early embryonic stage, which resembles the role the CMZ plays in the light-guided growth of the chicken retina (Fischer et al., 2013).

As SCF/SCFR signaling broadly involved with the early development of embryonic eye, the downstream target of the SCF/SCFR signaling pathway should be investigated. For retinal neurogenesis, the mTOR pathway could be an intriguing downstream target as it has been proved to be involved in neurogenesis in both the CMZ and central NR in lower vertebrates (Choi et al., 2018; Love et al., 2014; Saxton and Sabatini, 2017; Zelinka et al., 2016). The consequences of overactivation and inhibition of SCF/SCFR signaling differed between neurogenesis and gliogenesis in the central NR. These data suggest that SCF/SCFR signaling may be involved in modulation of an intrinsic retinal developmental gene such as *Lhx2* (de Melo et al., 2018). Other classic pathways of neural development, such as Wnt, Notch and Hedgehog signaling, may also crosstalk with SCF/SCFR signaling, as reported in other organ development or disease pathophysiology (Ahmad et al., 2004). The regulation of the SCFR itself is also an interesting topic. As the previous report found, AP2 α , the transcription factor that binds the promoter of the SCFR gene, plays a crucial role in the development of the optic stalk and the lens, and in OC patterning in the developing retina (Bassett et al., 2010; West-Mays et al., 1999). The basic helix-loop-helix transcription factor microphthalmia-associated transcription factor (MITF), which is the key marker of RPE development, is an important regulator of SCFR expression in mast cells and melanocytes (Opdecamp et al., 1997; Tsujimura et al., 1996). Interestingly, there is also an inverse regulation in that SCFR signaling regulates MITF expression through miRNAs miR-539 and miR-381 (Lee et al., 2011). Combined with the specific expression of the SCFR in the MITF-negative peripheral NR, which is tightly adjacent to the MITF-positive RPE, we predict that an interesting relationship could exist between the SCFR and MITF in this hinge-like region of optic cup.

To summarize, as an extrinsic environmental signal, SCF/SCFR signaling might serve as one of the mechanisms by which tissue-tissue interactions could be used in eye development (Fig. 7). However, lots of problems need to be explored in the field. Does the SCF/SCFR signaling involve the epithelial flow into the OC (Heermann et al., 2015) during the eye morphogenesis? Does the

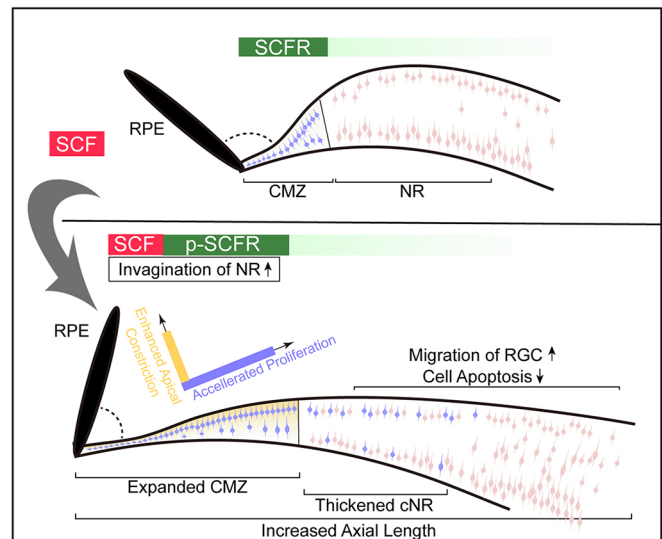


Fig. 7. Schematic of the developmental role of SCF/SCFR signaling in the human embryonic neural retina. Activation of SCF/SCFR signaling provided a tangential power, which derived from the rapid proliferation of RSC/RPCs in the CMZ, and a vertical (centrifugal) power generated by the enhanced apical constriction. These powers pull the NR toward the rigid RPE and facilitate the invagination of the NR. At the nonmarginal NR region, SCF promoted the migration of immature ganglion cells toward the basal side of the NR and repressed cell apoptosis in the NR, thus producing a pro-neurogenic effect during the early development of human embryonic neural retina.

expression of the SCFR differ from the different ocular axis during the early development of eye? What is the regulatory molecular mechanism of SCFR expression dynamics in the developing retina? In the future, answering these questions will be of great importance for better understanding human eye development and congenital eye disease.

MATERIALS AND METHODS

Human embryonic stem cell culture

All experiments were performed in accordance with the guidelines of the Ethics Committee of Southwest Hospital, The Army Medical University (Chongqing, PR China). The hESC Line H1 (RRID:CVCL_9771) was used in this research. Briefly, hESCs were cultured under feeder-free condition using Essential 8 Medium (Gibco) and Vitronectin (Gibco). For routine culture, hESC colonies were passaged every ~4-5 days using Versene (Gibco) at 37°C for 5 min. The detached hESC clumps were broken into small pieces by gentle pipetting. Morphologically identifiable differentiated cells were mechanically removed at each passage.

Retinal differentiation of hESCs and administration of SCF and isck03

The 3D human OC culture (SFEBq culture) was performed as previously described (Kuwahara et al., 2015). hESCs were dissociated into single cells in TrypLE Express (Gibco) and quickly reaggregated using low-cell adhesion 96-well plates with V-bottomed conical wells (Sumitomo Bakelite) in 3D OC differentiation medium (10,000 cells per well) supplemented with 20 mM Y-27632 (Sigma-Aldrich) under 5% CO₂ at 37°C. The differentiation medium contained 45% Iscove's modified Dulbecco's medium (IMDM, Gibco), 45% Hams F12 (F12, Gibco), Glutamax, 1% chemically defined lipid concentrate (Gibco), 10% knockout serum replacement (KSR) (Gibco), monoethyglycerol (450 μ M, Sigma-Aldrich), 100 U ml⁻¹ penicillin and 100 μ g ml⁻¹ streptomycin (Gibco). Recombinant human BMP4 (PeproTech) was added to the culture at a final concentration of 1.5 nM (55 ng/ml) on D6, and half of the medium was changed every 3rd day. The 3D retinal organoids were transferred to 9 cm Petri dishes (ultra-low adhesion, Corning) at D18 for further culture in suspension with long-term culture

medium containing DMEM/F12-Glutamax medium (Gibco), 1% N2 supplement (Gibco), 10% fetal bovine serum (FBS), 0.5 μM retinoic acid (Sigma-Aldrich), 0.1 mM taurine (Sigma-Aldrich), 0.25 $\mu\text{g ml}^{-1}$ fungizone (Gibco), 100 U ml^{-1} penicillin and 100 $\mu\text{g ml}^{-1}$ streptomycin (Gibco). Standard 3D OCs with both the NR and the RPE at D24 were collected in the experimental groups. Recombinant human SCF (R&D) and isck03 (Abcam) was added to the 3D culture at ~D24-D30 at a final concentration of 20 ng/ml and 100 μM , respectively.

BrdU-labeling assay

BrdU labeling was performed over different time courses, as indicated in the results. 3D OCs were cultured in long-term culture medium in the presence of BrdU (5 $\mu\text{g ml}^{-1}$, 16 μM ; Sigma-Aldrich). Aggregates were then washed with medium and cultured in the absence of BrdU for the BrdU dilution experiment or directly fixed for the BrdU incorporation experiment.

Immunofluorescence and confocal microscopy

Immunofluorescence was performed as previously described (Lakowski et al., 2018). Retinal organoids and human fetal retinae were fixed in 4% (wt/vol) phosphate-buffered formaldehyde solution at 4°C for 15–30 min, washed three times with PBS and equilibrated in 30% (wt/vol) sucrose solution at 4°C overnight. Specimens were then transferred into optimal cutting temperature (OCT) compound (Biosharp) and frozen at -80°C . A Leica CM1900UV cryostat was used to produce 10 μm sections. For immunofluorescence analysis, OCT compound was removed by a 15 min incubation at 37°C with PBS, and cryosections were blocked with 10% (vol/vol) FBS and 1% (wt/vol) bovine serum albumin (BSA) in PBS containing 0.1% (vol/vol) Triton X-100 for 1 h at room temperature. The following primary antibodies were used in the same blocking solution for 1 h at room temperature or overnight at 4°C: Rax (1:500; Abcam, ab23340), MITF (1:400; Abcam, ab3201), Pax6 (1:500; Abcam, ab78545), Chx10 (1:500; Abcam, ab93715), Sox2 (1:500; Abcam, ab97959), SSEA4 (1:500; Abcam, ab16287), Ki67 (1:500; Cell Signaling Technology, 9129), Nestin (1:200; Sigma-Aldrich, N5413), p27Kip1 (1:500; Abcam, ab32034), SSEA1 (1:400; Cell Signaling Technology, 4744S), AQP1 (1:500; Novus, NB600-749), SCFR (1:400; Cell Signaling Technology, 3308), BrdU (1:100; Sigma-Aldrich, B8434), pMLC (1:200; Abcam, ab2480), ZO-1 (1:400; Cell Signaling Technology, 13663), phalloidin (1:500; Sigma-Aldrich, P5282), Brn3b (1:200; Abcam, ab56026), Tuj1 (1:200; Cell Signaling Technology, 4466), cleaved-caspase 3 (1:500; Cell Signaling Technology, 9664), islet 1 (1:500; Abcam, ab109517), SCF (1:400; Abcam, ab52603), p-SCFR (1:300; Abcam, ab62154), Vsx2 (1:1000; Sigma-Aldrich, HPA003436), calretinin (1:1000; Millipore, MAB1568) and CRALBP (1:400; Abcam, ab15051). The primary antibody was omitted for negative controls. Primary antibody staining was followed by three washes with 1 \times PBS. Subsequently, cryosections were incubated for 1 h at room temperature with the appropriate secondary antibody (goat anti-rabbit Alexa Fluor 488, Invitrogen; goat anti-rabbit Alexa Fluor 594, Invitrogen; goat anti-mouse Alexa Fluor 488, Invitrogen; goat anti-mouse Alexa Fluor 594, Invitrogen; all 1:1000) diluted in blocking solution. DAPI (1:10, Beyotime) was applied for 10 min at room temperature to counterstain nuclei, followed by three washes with PBS prior to cover-slipping with the antifade mounting medium (Beyotime).

Microscopy, image acquisition and processing

A Zeiss LSM880 was used for the acquisition of confocal images. Images were processed in Zen2.3 (blue edition, Zeiss), FIJI, Photoshop CC 2017 (Adobe) and Illustrator CC 2017 (Adobe).

Quantification of the RPE-NR angle, the axial length and the CMZ length

A Leica DMI3000 was used for the acquisition of bright-field images of 3D retinal organoids. The NR-RPE angle, the axial length and the CMZ length were measured using ImageJ as indicated in Fig. 3A,D. The length of CMZ was defined as the distance between the RPE-NR boundary and the position where the inner cell layer emerges (the low gray value region of central NR in the bright field).

Real-time polymerase chain reaction (RT-PCR)

Three independent *in vitro* experiments were performed. Briefly, total RNA was extracted from 3D human OCs with TRIzol reagent (Gibco), and RNA was reverse-transcribed using the PrimeScript RT Reagent Kit (Takara). The cDNA was amplified with specific gene primers. Quantitative RT-PCR was conducted using the CFX96 Real-Time PCR System (Bio-Rad) with at least three separate RNA samples. Primers were as follows: Rax forward, AACCGCAGACTTTCACCAC; Rax reverse, TGCAGCTTCATGGAGGACAC; Lhx2 forward, GCGATGCTGTTCACAGTCT; Lhx2 reverse, TAGCGGTCCGAGATCTTGCC; Pax6 forward, CCAGGGCAATCGGTGGTAGT; Pax6 reverse, GCTAGCCAGGTTGCGAAGAA; Oct4 forward, GACAGGGGGAGGGGAGGAGCTAGG; Oct4 reverse, CTTCCCTCC-AACCAGTTGCCCAAAC; Sox2 forward, TTACGCGCACATGAACGGCT; Sox2 reverse, TCGGAGTAGGACATGCTGTA; SCFR forward, TCCCAGAGCCCAATAG; SCFR reverse, GAAGCTTGCCACATCG; GAPDH forward, CCATGTTGTCATGGGTGTGA, GAPDH reverse CATGAGTCCTCCACGATACCA.

Statistical analysis

Data are presented as means \pm s.e.m. Statistical tests were performed with the PRISM software (GraphPad, version 6.01). Statistical significance was tested with Student's *t*-test (parametric) and ANOVA with Tukey's or Dunnett's correction for multiple comparisons. A $P < 0.05$ was considered significant.

Acknowledgments

We thank Prof. Congjian Zhao, Mr Fei Ni, Dr Wenyi liu, Dr Yan Fu, Dr Mingming Liu, Dr Jiaman Dai and Miss Xi Chen for their kindly assistance in the early research.

Competing interests

The authors declare no competing or financial interests.

Author contributions

Conceptualization: Y.G., H.X.; Methodology: Y.G., X.H., Q.L., J.H., Y.L.; Software: Y.G., X.H.; Validation: L.G.; Formal analysis: Y.G., B.B., Y.L.; Investigation: Y.G., X.H.; Resources: Q.L., L.G., Y.Z.; Data curation: B.B.; Writing - original draft: Y.G.; Writing - review & editing: H.X., Z.Q.Y.; Visualization: Y.G.; Supervision: H.X., Z.Q.Y.; Project administration: H.X., Z.Q.Y.; Funding acquisition: H.X., Z.Q.Y.

Funding

This study was supported by funding from the Military Key Program (BWS13C015), the National Key R&D program of China (2018YFA0107302), the National Basic Research Program of China (2013CB967002) and National Natural Science Foundation of China (81873688). The funding bodies had no role in study design, in the collection, analysis or interpretation of data, in the writing of the report, or in the decision to submit the paper for publication.

Supplementary information

Supplementary information available online at <http://dev.biologists.org/lookup/doi/10.1242/dev.174409.supplemental>

References

- Agathocleous, M. and Harris, W. A. (2009). From progenitors to differentiated cells in the vertebrate retina. *Annu. Rev. Cell Dev. Biol.* **25**, 45–69. doi:10.1146/annurev.cellbio.042308.113259
- Ahmad, I., Das, A. V., James, J., Bhattacharya, S. and Zhao, X. (2004). Neural stem cells in the mammalian eye: types and regulation. *Semin. Cell Dev. Biol.* **15**, 53–62. doi:10.1016/j.semcdb.2003.09.003
- Bassett, E. A. and Wallace, V. A. (2012). Cell fate determination in the vertebrate retina. *Trends Neurosci.* **35**, 565–573. doi:10.1016/j.tins.2012.05.004
- Bassett, E. A., Williams, T., Zacharias, A. L., Gage, P. J., Fuhrmann, S. and West-Mays, J. A. (2010). AP-2alpha knockout mice exhibit optic cup patterning defects and failure of optic stalk morphogenesis. *Hum. Mol. Genet.* **19**, 1791–1804. doi:10.1093/hmg/ddq060
- Bélanger, M.-C., Robert, B. and Cayouette, M. (2017). Msx1-positive progenitors in the retinal ciliary margin give rise to both neural and non-neural progenies in mammals. *Dev. Cell* **40**, 137–150. doi:10.1016/j.devcel.2016.11.020
- Cayouette, M. and Raff, M. (2003). The orientation of cell division influences cell-fate choice in the developing mammalian retina. *Development* **130**, 2329–2339. doi:10.1242/dev.00446
- Cayouette, M., Poggi, L. and Harris, W. A. (2006). Lineage in the vertebrate retina. *Trends Neurosci.* **29**, 563–570. doi:10.1016/j.tins.2006.08.003

- Chen, S., Li, H., Gaudenz, K., Paulson, A., Guo, F., Trimble, R., Peak, A., Seidel, C., Deng, C., Furuta, Y. et al. (2013). Defective FGF signaling causes coloboma formation and disrupts retinal neurogenesis. *Cell Res.* **23**, 254-273. doi:10.1038/cr.2012.150
- Chen, X., Chen, Z., Li, Z., Zhao, C., Zeng, Y., Zou, T., Fu, C., Liu, X., Xu, H. and Yin, Z. Q. (2016). Grafted c-kit+/SSEA1- eye-wall progenitor cells delay retinal degeneration in mice by regulating neural plasticity and forming new graft-to-host synapses. *Stem Cell Res Ther.* **7**, 191. doi:10.1186/s13287-016-0451-8
- Choi, J.-H., Jo, H. S., Lim, S., Kim, H.-T., Lee, K. W., Moon, K. H., Ha, T., Kwak, S. S., Kim, Y., Lee, E. J. et al. (2018). mTORC1 accelerates retinal development via the immunoproteasome. *Nat. Commun.* **9**, 2502. doi:10.1038/s41467-018-04774-9
- Das, T., Payer, B., Cayouette, M. and Harris, W. A. (2003). In vivo time-lapse imaging of cell divisions during neurogenesis in the developing zebrafish retina. *Neuron* **37**, 597-609. doi:10.1016/S0896-6273(03)00066-7
- Das, A. V., Edakkot, S., Thoreson, W. B., James, J., Bhattacharya, S. and Ahmad, I. (2005a). Membrane properties of retinal stem cells/progenitors. *Prog. Retin. Eye Res.* **24**, 663-681. doi:10.1016/j.preteyeres.2005.04.003
- Das, A. V., James, J., Rahnenführer, J., Thoreson, W. B., Bhattacharya, S., Zhao, X. and Ahmad, I. (2005b). Retinal properties and potential of the adult mammalian ciliary epithelium stem cells. *Vision Res.* **45**, 1653-1666. doi:10.1016/j.visres.2004.12.017
- de Melo, J., Clark, B. S. and Venkataraman, A. (2018). Ldb1- and Rnf12-dependent regulation of Lhx2 controls the relative balance between neurogenesis and gliogenesis in the retina. *Development* **145**, dev159970. doi:10.1242/dev.159970
- Dyer, M. A. and Cepko, C. L. (2001). p27Kip1 and p57Kip2 regulate proliferation in distinct retinal progenitor cell populations. *J. Neurosci.* **21**, 4259-4271. doi:10.1523/JNEUROSCI.21-12-04259.2001
- Eiraku, M., Takata, N., Ishibashi, H., Kawada, M., Sakakura, E., Okuda, S., Sekiguchi, K., Adachi, T. and Sasai, Y. (2011). Self-organizing optic-cup morphogenesis in three-dimensional culture. *Nature* **472**, 51-56. doi:10.1038/nature09941
- Eiraku, M., Adachi, T. and Sasai, Y. (2012). Relaxation-expansion model for self-driven retinal morphogenesis: a hypothesis from the perspective of biosystems dynamics at the multi-cellular level. *BioEssays* **34**, 17-25. doi:10.1002/bies.201100070
- Fischer, A. J., Bosse, J. L. and El-Hodiri, H. M. (2013). The ciliary marginal zone (CMZ) in development and regeneration of the vertebrate eye. *Exp. Eye Res.* **116**, 199-204. doi:10.1016/j.exer.2013.08.018
- Fuhrmann, S. (2010). Eye morphogenesis and patterning of the optic vesicle. *Curr. Top. Dev. Biol.* **93**, 61-84. doi:10.1016/B978-0-12-385044-7.00003-5
- Guijarran, P., Wang, Y., Ying, Y., Yao, Y., Jieyi, X. and Yuan, X. (2013). In vivo knockdown of cKit impairs neuronal migration and axonal extension in the cerebral cortex. *Dev. Neurobiol.* **73**, 871-887. doi:10.1002/dneu.22107
- Harris, W. A. and Perron, M. (1998). Molecular recapitulation: the growth of the vertebrate retina. *Int. J. Dev. Biol.* **42**, 299-304.
- Hasegawa, T., McLeod, D. S., Prow, T., Merges, C., Grebe, R. and Luty, G. A. (2008). Vascular precursors in developing human retina. *Invest. Ophthalmol. Vis. Sci.* **49**, 2178-2192. doi:10.1167/iovs.07-0632
- Heavner, W. and Pevny, L. (2012). Eye development and retinogenesis. *Cold Spring Harb Perspect Biol.* **4**, a008391. doi:10.1101/cshperspect.a008391
- Heermann, S., Schutz, L., Lemke, S., Krieglstein, K. and Wittbrodt, J. (2015). Eye morphogenesis driven by epithelial flow into the optic cup facilitated by modulation of bone morphogenetic protein. *Elife* **4**, e05216. doi:10.7554/eLife.05216
- Heinrich, M. C., Blanke, C. D., Druker, B. J. and Corless, C. L. (2002). Inhibition of KIT tyrosine kinase activity: a novel molecular approach to the treatment of KIT-positive malignancies. *J. Clin. Oncol.* **20**, 1692-1703. doi:10.1200/JCO.2002.20.6.1692
- Hirota, S., Isozaki, K., Moriyama, Y., Hashimoto, K., Nishida, T., Ishiguro, S., Kawano, K., Hanada, M., Kurata, A., Takeda, M. et al. (1998). Gain-of-function mutations of c-kit in human gastrointestinal stromal tumors. *Science* **279**, 577-580. doi:10.1126/science.279.5350.577
- Hoshino, A., Ratnapriya, R., Brooks, M. J., Chaitankar, V., Wilken, M. S., Zhang, C., Starostik, M. R., Gieser, L., La Torre, A., Nishio, M. et al. (2017). Molecular anatomy of the developing human retina. *Dev. Cell* **43**, 763-779.e764. doi:10.1016/j.devcel.2017.10.029
- Keshet, E., Lyman, S. D., Williams, D. E., Anderson, D. M., Jenkins, N. A., Copeland, N. G. and Parada, L. F. (1991). Embryonic RNA expression patterns of the c-kit receptor and its cognate ligand suggest multiple functional roles in mouse development. *EMBO J.* **10**, 2425-2435. doi:10.1002/j.1460-2075.1991.tb07782.x
- Koso, H., Satoh, S. and Watanabe, S. (2007). c-kit marks late retinal progenitor cells and regulates their differentiation in developing mouse retina. *Dev. Biol.* **301**, 141-154. doi:10.1016/j.ydbio.2006.09.027
- Koso, H., Iida, A., Tabata, Y., Baba, Y., Satoh, S., Taketo, M. M. and Watanabe, S. (2008). CD138/syndecan-1 and SSEA-1 mark distinct populations of developing ciliary epithelium that are regulated differentially by Wnt signal. *Stem Cells* **26**, 3162-3171. doi:10.1634/stemcells.2008-0303
- Kuwahara, A., Ozone, C., Nakano, T., Saito, K., Eiraku, M. and Sasai, Y. (2015). Generation of a ciliary margin-like stem cell niche from self-organizing human retinal tissue. *Nat. Commun.* **6**, 6286. doi:10.1038/ncomms7286
- Lakowski, J., Welby, E., Budinger, D., Di Marco, F., Di Foggia, V., Bainbridge, J. W. B., Wallace, K. and Gamm, D. M. (2018). Isolation of human photoreceptor precursors via a cell surface marker panel from stem cell-derived retinal organoids and fetal retinae. *Stem Cells* **36**, 709-722. doi:10.1002/stem.2775
- Larsen, K. B., Lutterodt, M., Rath, M. F. and Moller, M. (2009). Expression of the homeobox genes PAX6, OTX2, and OTX1 in the early human fetal retina. *Int. J. Dev. Neurosci.* **27**, 485-492. doi:10.1016/j.ijdevneu.2009.04.004
- Lee, Y.-N., Brandal, S., Noel, P., Wentzel, E., Mendell, J. T., McDevitt, M. A., Kapur, R., Carter, M., Metcalfe, D. D. and Takemoto, C. M. (2011). KIT signaling regulates MITF expression through miRNAs in normal and malignant mast cell proliferation. *Blood* **117**, 3629-3640. doi:10.1182/blood-2010-07-293548
- Lennartsson, J. and Rönstrand, L. (2012). Stem cell factor receptor/c-Kit: from basic science to clinical implications. *Physiol. Rev.* **92**, 1619-1649. doi:10.1152/physrev.00046.2011
- Livesey, F. J. and Cepko, C. L. (2001). Vertebrate neural cell-fate determination: lessons from the retina. *Nat. Rev. Neurosci.* **2**, 109-118. doi:10.1038/35053522
- Love, N. K., Keshavan, N., Lewis, R., Harris, W. A. and Agathocleous, M. (2014). A nutrient-sensitive restriction point is active during retinal progenitor cell differentiation. *Development* **141**, 697-706. doi:10.1242/dev.103978
- Lowe, A., Harris, R., Bhansali, P., Cvekl, A. and Liu, W. (2016). Intercellular adhesion-dependent cell survival and ROCK-regulated actomyosin-driven forces mediate self-formation of a retinal organoid. *Stem Cell Reports.* **6**, 743-756. doi:10.1016/j.stemcr.2016.03.011
- Matsui, Y., Zsebo, K. M. and Hogan, B. L. (1990). Embryonic expression of a haematopoietic growth factor encoded by the Sl locus and the ligand for c-kit. *Nature* **347**, 667-669. doi:10.1038/347667a0
- Mellough, C. B. and Bauer, R. (2019). An integrated transcriptional analysis of the developing human retina. *Development* **146**, dev169474. doi:10.1242/dev.169474
- Mellough, C. B., Collin, J., Khazim, M., White, K., Sernagor, E., Steel, D. H. and Lako, M. (2015). IGF-1 signaling plays an important role in the formation of three-dimensional laminated neural retina and other ocular structures from human embryonic stem cells. *Stem Cells* **33**, 2416-2430. doi:10.1002/stem.2023
- Nakano, T., Ando, S., Takata, N., Kawada, M., Mugeruma, K., Sekiguchi, K., Saito, K., Yonemura, S., Eiraku, M. and Sasai, Y. (2012). Self-formation of optic cups and storable stratified neural retina from human ESCs. *Cell Stem Cell.* **10**, 771-785. doi:10.1016/j.stem.2012.05.009
- Oakie, A., Feng, Z.-C., Li, J., Silverstein, J., Yee, S.-P. and Wang, R. (2019). Long-term c-Kit overexpression in beta cells compromises their function in ageing mice. *Diabetologia* **62**, 1430-1444. doi:10.1007/s00125-019-4890-5
- O'Brien, K. M., Schulte, D. and Hendrickson, A. E. (2003). Expression of photoreceptor-associated molecules during human fetal eye development. *Mol. Vis.* **9**, 401-409.
- Opdecamp, K., Nakayama, A., Nguyen, M. T., Hodgkinson, C. A., Pavan, W. J. and Arnheiter, H. (1997). Melanocyte development in vivo and in neural crest cell cultures: crucial dependence on the Mitf basic-helix-loop-helix-zipper transcription factor. *Development* **124**, 2377-2386.
- Paşca, S. P. (2018). The rise of three-dimensional human brain cultures. *Nature* **553**, 437-445. doi:10.1038/nature25032
- Picker, A. and Brand, M. (2005). Fgf signals from a novel signaling center determine axial patterning of the prospective neural retina. *Development* **132**, 4951-4962. doi:10.1242/dev.02071
- Pilaz, L.-J., McMahon, J. J., Miller, E. E., Lennox, A. L., Suzuki, A., Salmon, E. and Silver, D. L. (2016). Prolonged mitosis of neural progenitors alters cell fate in the developing brain. *Neuron* **89**, 83-99. doi:10.1016/j.neuron.2015.12.007
- Rossi, G., Manfrin, A. and Lutolf, M. P. (2018). Progress and potential in organoid research. *Nat. Rev. Genet.* **19**, 671-687. doi:10.1038/s41576-018-0051-9
- Sasai, Y. (2013). Cytosystems dynamics in self-organization of tissue architecture. *Nature* **493**, 318-326. doi:10.1038/nature11859
- Saxton, R. A. and Sabatini, D. M. (2017). mTOR signaling in growth, metabolism, and disease. *Cell* **168**, 960-976. doi:10.1016/j.cell.2017.02.004
- Sun, L., Lee, J. and Fine, H. A. (2004). Neuronally expressed stem cell factor induces neural stem cell migration to areas of brain injury. *J. Clin. Invest.* **113**, 1364-1374. doi:10.1172/JCI200420001
- Teng, X. and Toyama, Y. (2011). Apoptotic force: active mechanical function of cell death during morphogenesis. *Dev. Growth Differ.* **53**, 269-276. doi:10.1111/j.1440-169X.2011.01251.x
- Toyama, Y., Peralta, X. G., Wells, A. R., Kiehart, D. P. and Edwards, G. S. (2008). Apoptotic force and tissue dynamics during Drosophila embryogenesis. *Science* **321**, 1683-1686. doi:10.1126/science.1157052
- Tsujiyama, T., Morii, E., Nozaki, M., Hashimoto, K., Moriyama, Y., Takebayashi, K., Kondo, T., Kanakura, Y. and Kitamura, Y. (1996). Involvement of transcription factor encoded by the mi locus in the expression of c-kit receptor tyrosine kinase in cultured mast cells of mice. *Blood* **88**, 1225-1233.
- Valdivia, L. E., Lamb, D. B., Horner, W., Wierzbicki, C., Tafessu, A., Williams, A. M., Gestri, G., Krasnow, A. M., Vleeshouwer-Neumann, T. S., Givens, M. et al. (2016). Antagonism between Gdf6a and retinoic acid pathways controls

- timing of retinal neurogenesis and growth of the eye in zebrafish. *Development* **143**, 1087-1098. doi:10.1242/dev.130922
- Vecino, E. and Acera, A.** (2015). Development and programmed cell death in the mammalian eye. *Int. J. Dev. Biol.* **59**, 63-71. doi:10.1387/ijdb.150070ev
- Wang, H., Zhuang, X., Cai, Y., Cheung, A. Y. and Jiang, L.** (2013). Apical F-actin-regulated exocytic targeting of NtPPME1 is essential for construction and rigidity of the pollen tube cell wall. *Plant J.* **76**, 367-379. doi:10.1111/tpj.12300
- West-Mays, J. A., Zhang, J., Nottoli, T., Hagopian-Donaldson, S., Libby, D., Strissel, K. J. and Williams, T.** (1999). AP-2alpha transcription factor is required for early morphogenesis of the lens vesicle. *Dev. Biol.* **206**, 46-62. doi:10.1006/dbio.1998.9132
- Woodman, S. E. and Davies, M. A.** (2010). Targeting KIT in melanoma: a paradigm of molecular medicine and targeted therapeutics. *Biochem. Pharmacol.* **80**, 568-574. doi:10.1016/j.bcp.2010.04.032
- Xu, H., Yang, Y., Tang, X., Zhao, M., Liang, F., Xu, P., Hou, B., Xing, Y., Bao, X. and Fan, X.** (2013). Bergmann glia function in granule cell migration during cerebellum development. *Mol. Neurobiol.* **47**, 833-844. doi:10.1007/s12035-013-8405-y
- Xu, L., Tang, X., Wang, Y., Xu, H. and Fan, X.** (2015). Radial glia, the keystone of the development of the hippocampal dentate gyrus. *Mol. Neurobiol.* **51**, 131-141. doi:10.1007/s12035-014-8692-y
- Xue, X. Y. and Harris, W. A.** (2012). Using myc genes to search for stem cells in the ciliary margin of the *Xenopus* retina. *Dev. Neurobiol.* **72**, 475-490. doi:10.1002/dneu.20887
- Yamaguchi, Y., Watanabe, T., Hirakata, A. and Hida, T.** (2006). Localization and ontogeny of aquaporin-1 and -4 expression in iris and ciliary epithelial cells in rats. *Cell Tissue Res.* **325**, 101-109. doi:10.1007/s00441-005-0122-z
- Zelinka, C. P., Volkov, L., Goodman, Z. A., Todd, L., Palazzo, I., Bishop, W. A. and Fischer, A. J.** (2016). mTor signaling is required for the formation of proliferating Müller glia-derived progenitor cells in the chick retina. *Development* **143**, 1859-1873. doi:10.1242/dev.133215
- Zhong, W. and Chia, W.** (2008). Neurogenesis and asymmetric cell division. *Curr. Opin. Neurobiol.* **18**, 4-11. doi:10.1016/j.conb.2008.05.002
- Zhong, X., Gutierrez, C., Xue, T., Hampton, C., Vergara, M. N., Cao, L.-H., Peters, A., Park, T. S., Zambidis, E. T., Meyer, J. S. et al.** (2014). Generation of three-dimensional retinal tissue with functional photoreceptors from human iPSCs. *Nat. Commun.* **5**, 4047. doi:10.1038/ncomms5047
- Zhou, P.-Y., Peng, G.-H., Xu, H. and Yin, Z. Q.** (2015). c-Kit(+) cells isolated from human fetal retinas represent a new population of retinal progenitor cells. *J. Cell Sci.* **128**, 2169-2178. doi:10.1242/jcs.169086
- Žigman, M., Cayouette, M., Charalambous, C., Schleiffer, A., Hoeller, O., Dunican, D., McCudden, C. R., Firnberg, N., Barres, B. A., Siderovski, D. P. et al.** (2005). Mammalian inscuteable regulates spindle orientation and cell fate in the developing retina. *Neuron* **48**, 539-545. doi:10.1016/j.neuron.2005.09.030
- Zou, T., Gao, L., Zeng, Y., Li, Q., Li, Y., Chen, S., Hu, X., Chen, X., Fu, C. and Xu, H.** (2019). Organoid-derived C-Kit(+)/SSEA4(-) human retinal progenitor cells promote a protective retinal microenvironment during transplantation in rodents. *Nat. Commun.* **10**, 1205. doi:10.1038/s41467-019-08961-0

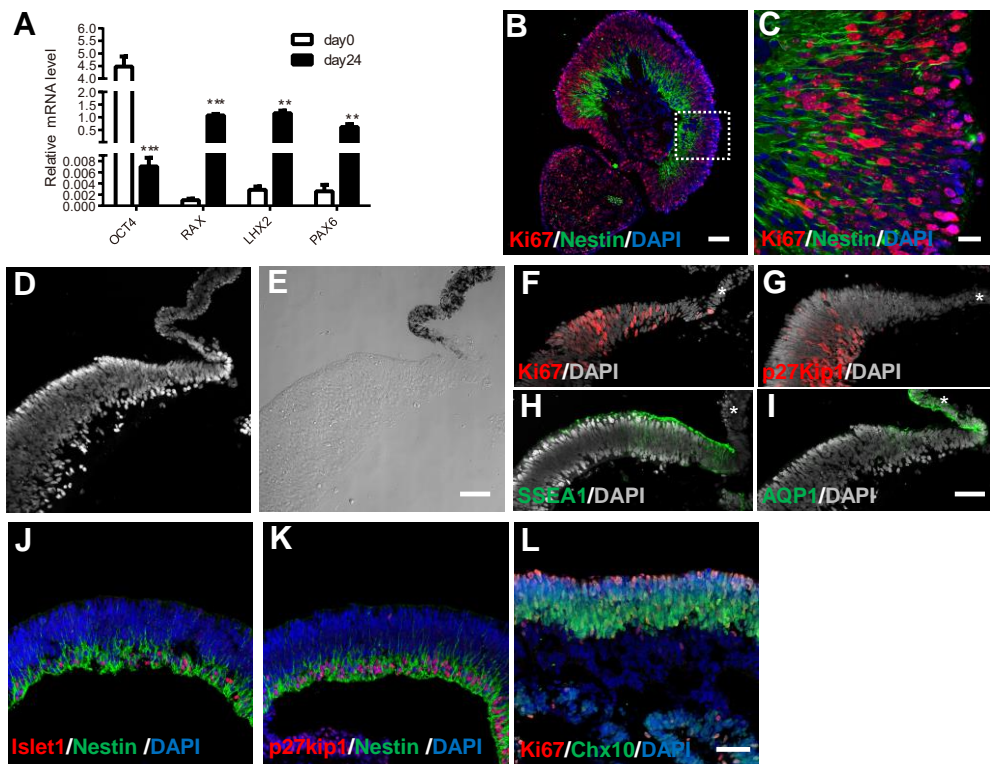


Figure S1. Identification and characteristics of the retinal organoid and CMZ. (A) RT-PCR analysis of mRNA of OCT4, Rax, LHX, and Pax6 in the 3D retinal organoid at D0 and D24. The pluripotent marker OCT4 was robustly downregulated after retinal differentiation while the eye field transcription factors Rax, LHX2, and Pax6 were dramatically upregulated after the formation of the 3D OC. (Mean \pm SD; D0, n=9; D24, n=9, 3 independent experiments) **p < 0.01; ***p < 0.005. (B,C) Immunostaining of 3D human retinal organoids at D24 for Nestin and Ki67. (D,E) DAPI staining and a differential interference contrast (DIC) image of the CMZ showing the specific cell shape and arrangement in the CMZ. (F~I) Immunostaining of the CMZ at D30 for Ki67 (F), P27kip1 (G), SSEA1 (H), and AQP1 (I). (J) Immunostaining of Islet1 and Nestin shows the Islet1⁺ ganglion progenitor cells were colocalized with Nestin at D24. (K) Nestin is expressed in the cell body of inner cell layer at D24 in which the CDK inhibitor p27Kip1 is present. (L) Ki67⁺ was distributed at the most apical layer of the uncommitted Chx10⁺ retinal progenitor cells. Scale bars: 20 μ m (C); 50 μ m (D~I), 100 μ m (B, J~L).

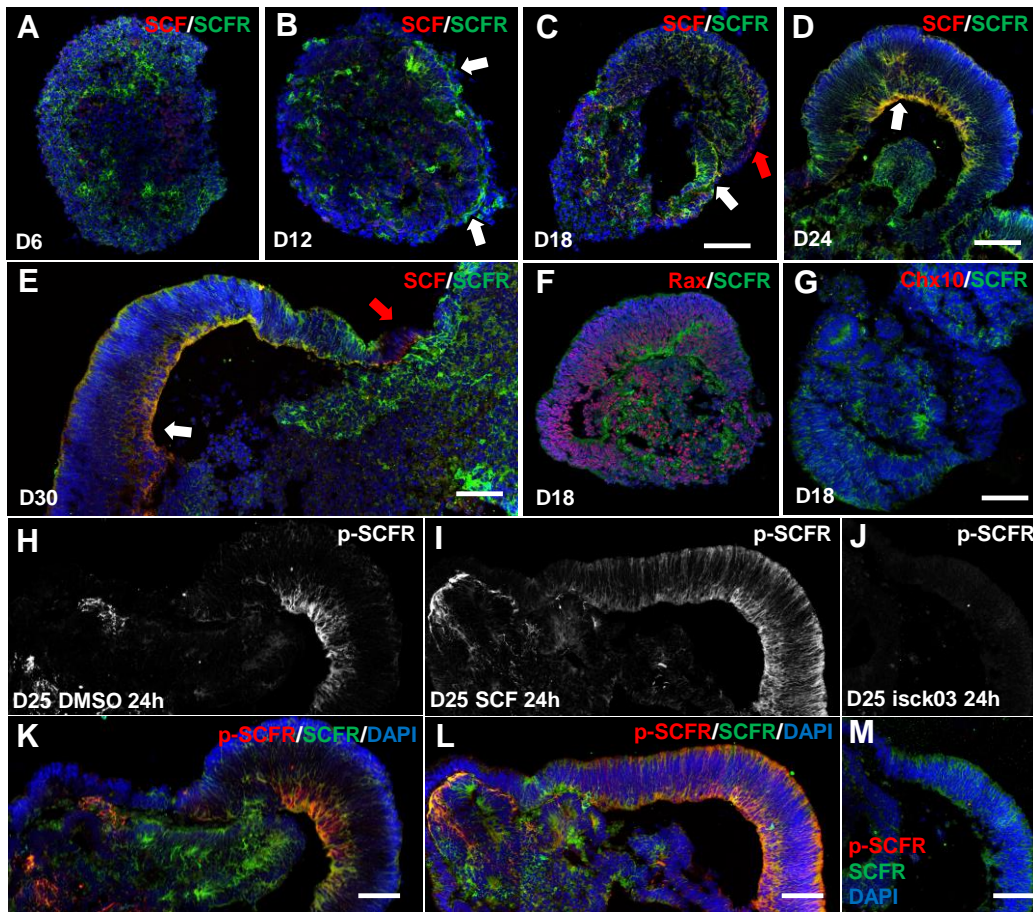


Figure S2. Spatiotemporal expression pattern of SCF and SCFR during the development of retinal organoid and activation of SCF/SCFR signaling pathway.

(A~E) SCFR first emerged at the outer portion of embryonic body at D6(A), gradually enriched at the epithelium-like tissue and cells at D12(B, white arrow), robustly located at the optic vesicle and neural retina at D18 and D24(C, D, white arrow), and preferentially maintained highly expressed in the CMZ and negatively expressed in the RPE at D30(E, white arrow). SCF was not expressed until D18 when the original optic vesicle formed(A~C, red arrow). Location of SCF mainly included two domain: basal side of the central SCFR positive NR and SCFR negative tissue(RPE), meanwhile hardly expressed in the CMZ(D, E, red arrow). (F~G) The Rax⁺ optic vesicle was first emerged at D18 when the neural retina marker Chx10 was not expressed yet. (H~M) p-SCFR signal robustly emerged in the basal side of the central NR at D25(H, K); p-SCFR was enhanced by SCF(I, L)and inhibit by isck03(J, M) Scale bars: 100 μ m (A~D, F, G); 200 μ m (E, H~M).

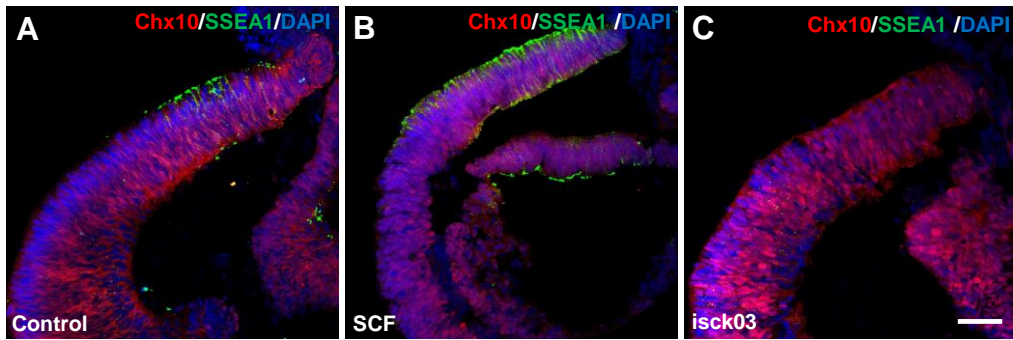


Figure S3. The border of CMZ and NR delimited by the staining of SSEA1 and Chx10. (A~C) Double-staining of SSEA1 and Chx10 in the control (A), SCF (B), and isck03 (C) treatment group at D30. Scale bars: 100 μ m (A~C)

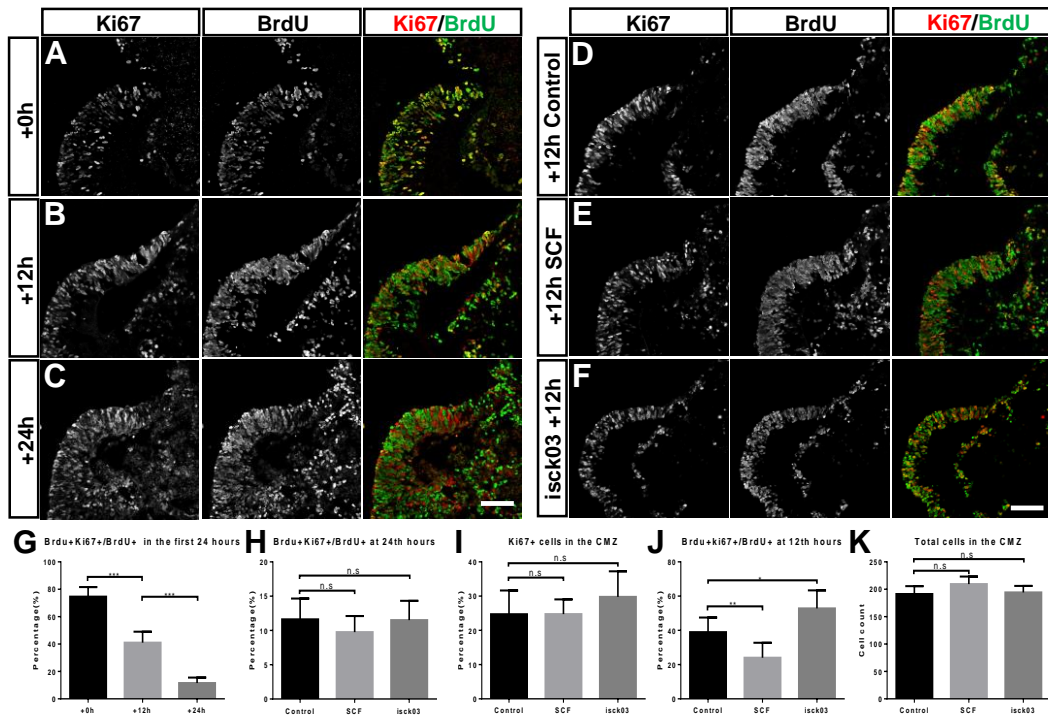


Figure S4. The SCF/SCFR signaling regulated the cell cycle progression of RPCs in the CMZ. (A~C) Double staining of BrdU and Ki67 at 0th, 12th, 24th hours BrdU incorporation. (D~F) Double staining of BrdU and Ki67 at an intermediate stage of cell cycle (12th hours after 24 hours BrdU incorporation) in the control, SCF, and isck03 treatment group. (G) The percentage of BrdU⁺/Ki67⁺ cells in the BrdU⁺ cells at different stage in the first 24 hours after BrdU incorporation. (H) The percentage of BrdU⁺/Ki67⁺ cells in the BrdU⁺ cells at the 24th hours after BrdU incorporation. (I) The percentage of Ki67⁺ cells in the total cells of CMZ after 24 hours of SCF or isck03 treatment. (J) The percentage of BrdU⁺/Ki67⁺ cells in the BrdU⁺ cells at the 12th hours after BrdU incorporation. (K) The cell count of all the cells in the CMZ at D30 after SCF or isck03 treatment. Data are shown as mean ± SEM. Independent sample t test.

*p < 0.05, **p < 0.01, ***p < 0.005, ****p < 0.0001. Scale bars: 200 μm (A~F).

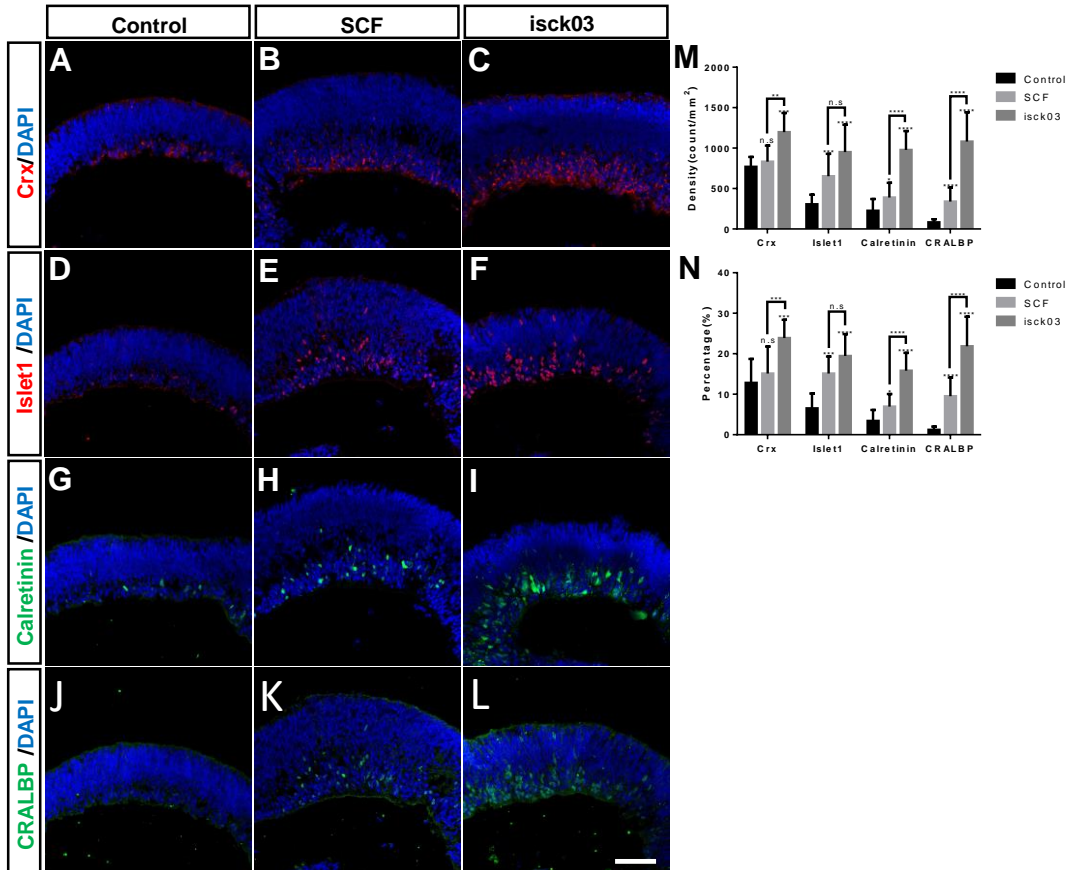


Figure S5. Imbalance of the SCF/SCFR signaling disturbed the early neurogenesis of NR. (A~L) Immunostaining of each cell type progenitor marker in the control, SCF, and isck03 group at D30: Crx (A~C, red), Islet1 (D~F, red), Calretinin (G~I, green), CRALBP (J~L, green). M~N, Statistics analysis of cell density and cell percent of each committed progenitor cells among the control, SCF, and isck03 group. Data are shown as mean \pm SD. Independent sample t test. * $p < 0.05$, ** $p < 0.01$, *** $p < 0.005$, **** $p < 0.0001$. Scale bars: 100 μ m (A~L).

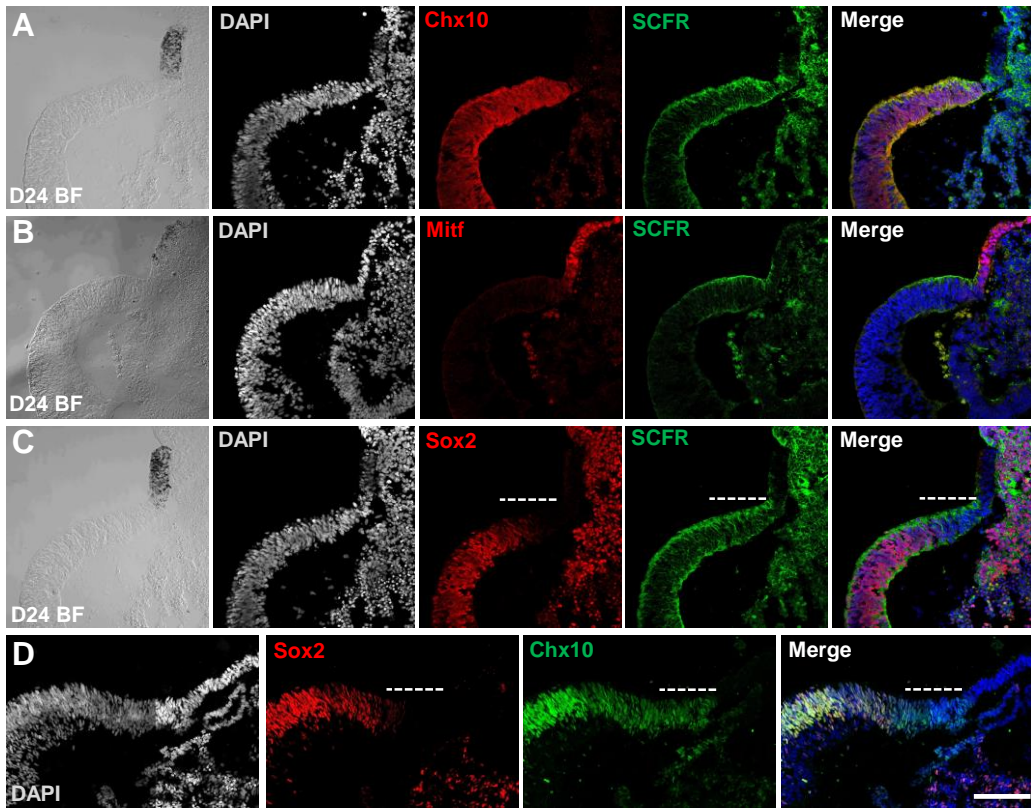


Figure S6. The heterogeneity of cells in the CMZ of human OC.

(A~C) Immunostaining of D24 retinal organoid shows overlapped distribution of SCFR and Chx10(A); distinctive distribution of SCFR and MITF(B); similar distribution of SCFR and Sox2(C). (D) Double staining of Chx10 and Sox2 at D24 shows the cell heterogeneity in the CMZ(dashed line: Chx10⁺Sox2⁻ region). Scale bars: 200 μm(A~D).